Received: 30 April 2024 | Revised: 19 July 2024 | Accepted: 24 July 2024

DOI: 10.1111/jnc.16197

Journal of Neurochemistry JNC The Official Journal of the International Society for Neurochemistry WILEY

ORIGINAL ARTICLE

A biallelic mutation in CACNA2D2 associated with developmental and epileptic encephalopathy affects calcium channel-dependent as well as synaptic functions of $\alpha_2\delta$-2

Sabrin Haddad[1,2] | Cornelia Ablinger[1,2] | Ruslan Stanika[2] | Manuel Hessenberger[2] | Marta Campiglio[1] | Nadine J. Ortner[3] | Petronel Tuluc[3] | Gerald J. Obermair[2]

[1]Institute of Physiology, Medical University Innsbruck, Innsbruck, Austria

[2]Division of Physiology, Department of Pharmacology, Physiology, and Microbiology, Karl Landsteiner University of Health Sciences, Krems, Austria

[3]Department of Pharmacology and Toxicology, University of Innsbruck, Innsbruck, Austria

Correspondence
Gerald J. Obermair, Division of Physiology, Department of Pharmacology, Physiology, and Microbiology, Karl Landsteiner University of Health Sciences, 3500 Krems, Austria.
Email: gerald.obermair@kl.ac.at

Funding information
Gesellschaft für Forschungsförderung Niederösterreich, Grant/Award Number: FTI22-D-013 and LSC19-017; Austrian Science Fund, Grant/Award Number: DOC178, DOC30, P31434, P35087 and P36053

Abstract

$\alpha_2\delta$ proteins serve as auxiliary subunits of voltage-gated calcium channels and regulate channel membrane expression and current properties. Besides their channel function, $\alpha_2\delta$ proteins regulate synapse formation, differentiation, and synaptic wiring. Considering these important functions, it is not surprising that CACNA2D1-4, the genes encoding for $\alpha_2\delta$-1 to -4 isoforms, have been implicated in neurological, neurodevelopmental, and neuropsychiatric disorders. Mutations in CACNA2D2 have been associated with developmental and epileptic encephalopathy (DEE) and cerebellar atrophy. In our present study, we performed a detailed functional characterization of the p.R593P mutation in $\alpha_2\delta$-2, a homozygous mutation previously identified in two siblings with DEE. Importantly, we analyzed both calcium channel-dependent as well as synaptic functions of $\alpha_2\delta$-2. Our data show that the corresponding p.R596P mutation in mouse $\alpha_2\delta$-2 drastically decreases membrane expression and synaptic targeting of $\alpha_2\delta$-2. This defect correlates with altered biophysical properties of postsynaptic $Ca_V1.3$ channel but has no effect on presynaptic $Ca_V2.1$ channels upon heterologous expression in tsA201 cells. However, homologous expression of $\alpha_2\delta$-2_R596P in primary cultures of hippocampal neurons affects the ability of $\alpha_2\delta$-2 to induce a statistically significant increase in the presynaptic abundance of endogenous $Ca_V2.1$ channels and presynaptic calcium transients. Moreover, our data demonstrate that in addition to lowering membrane expression, the p.R596P mutation reduces the trans-synaptic recruitment of $GABA_A$ receptors and presynaptic synapsin clustering in glutamatergic synapses. Lastly, the $\alpha_2\delta$-2_R596P reduces the amplitudes of glutamatergic miniature postsynaptic currents in transduced hippocampal neurons. Taken together, our data strongly link the human biallelic p.R593P mutation to the

Abbreviations: Ca^{2+}, calcium; CACNA2D1–4, calcium channel auxiliary subunit alpha2delta-coding genes; Ca_V, voltage-gated calcium channels; CNS, central nervous system; DEE, developmental and epileptic encephalopathy; DIV, days in vitro; $GABA_AR$, $GABA_A$ receptor; HA, hemagglutinin; mEPSCs, miniature excitatory postsynaptic currents; MIDAS, metal ion-dependent adhesion site; RRID, Research Resource Identifier; VGCC, voltage-gated calcium channel; vGLUT1, vesicular glutamate transporter 1; VWA, von Willebrand factor type A domain; WT, wild type.

underlying severe neurodevelopmental disorder and highlight the importance of studying $\alpha_2\delta$ mutations not only in the context of channelopathies but also synaptopathies.

KEYWORDS
auxiliary subunit, calcium current, epilepsy, neurodevelopmental disorders, trans-synaptic function, voltage-gated calcium channels

1 | INTRODUCTION

Calcium (Ca^{2+}) entry into excitable cells is tightly regulated by voltage-gated Ca^{2+} channels (VGCCs, Ca_V). Neuronal channels of the Ca_V1 and Ca_V2 families are multimeric complexes consisting of pore-forming α_1 and two auxiliary subunits, β and $\alpha_2\delta$. Four genes encode for $\alpha_2\delta$ subunits (CACNA2D1-4) out of which three isoforms ($\alpha_2\delta$-1-3) are highly expressed in the central nervous system (CNS) (Schlick et al., 2010). The classical roles of $\alpha_2\delta$ proteins as auxiliary subunits of VGCCs, regulating the functional membrane expression and modulating the Ca^{2+} currents, are widely studied (reviewed in Dolphin, 2016). Recently, all four $\alpha_2\delta$ isoforms were recognized as important regulators of synaptic functions and these functions may be partially or entirely independent of the Ca^{2+} channel complex (reviewed in Dolphin & Obermair, 2022; Geisler et al., 2015). For example, loss of presynaptic $\alpha_2\delta$ subunits in murine cultured hippocampal neurons disrupted both pre- and postsynaptic differentiation, indicating that $\alpha_2\delta$ isoforms are necessary for glutamatergic synapse formation and trans-synaptic differentiation (Schopf et al., 2021). Moreover, altered expression levels of presynaptic $\alpha_2\delta$-1 and $\alpha_2\delta$-2 splice variants induce aberrant synaptic wiring and change the postsynaptic molecular composition by a trans-synaptic mechanism (Ablinger et al., 2022; Geisler et al., 2019). This emphasizes the importance of $\alpha_2\delta$ proteins in brain connectivity and suggests that aberrant expression of $\alpha_2\delta$ proteins may affect the excitatory–inhibitory balance. Therefore, it is not surprising that $\alpha_2\delta$ proteins have been implicated in various neurological disorders (reviewed in Ablinger et al., 2020; Ablinger et al., 2024; Hessenberger et al., 2023).

However, whether aberrant $\alpha_2\delta$ protein functions cause such defects by altered Ca^{2+} channel modulation, synaptic mechanism, or both is largely unknown. Several genes encoding VGCC subunits have been associated with epileptic encephalopathy, including CACNA1A (Epi, 2016; Epi et al., 2013; Niu et al., 2022), CACNA1C (Bozarth et al., 2018), CACNA1E (Helbig et al., 2018), CACNA2D1 (Dahimene et al., 2022), and CACNA2D2 (Table 1). The $\alpha_2\delta$-2 isoform is highly expressed in the cerebellum and is relevant for the structure and function of cerebellar synapses (Beeson et al., 2020; Beeson et al., 2021). Besides $\alpha_2\delta$-1, it is one of the targets of the highly prescribed anti-epileptic drugs pregabalin and gabapentin (Gong et al., 2001). To date, five cases of infantile-onset epilepsy and cerebellar atrophy linked to bi-allelic mutations in CACNA2D2 have been reported in unrelated families (Table 1; Butler et al., 2018; Edvardson et al., 2013; Pippucci et al., 2013; Punetha et al., 2019). The clinical presentation of all patients is strikingly similar to the phenotypes of ducky mutant mice, carrying a CACNA2D2 loss-of-function mutation, and $\alpha_2\delta$-2 knockout mice (Barclay et al., 2001; Brodbeck et al., 2002; Donato et al., 2006; Ivanov et al., 2004), strengthening the hypothesis that abnormal $\alpha_2\delta$-2 expression or function may underlie the epileptic phenotype for these patients. However, as of today, in-depth mechanistic analysis of these mutations is still missing and, if studied, limited to the so-called "channelopathies," essentially describing the consequences of $\alpha_2\delta$ mutations on Ca^{2+} channel functions (Edvardson et al., 2013).

To overcome this limitation, in this study, we aimed to characterize a previously reported rare homozygous missense variant (p.R593P) found in two siblings with developmental and epileptic encephalopathy (DEE) (Punetha et al., 2019) by studying the effects on the biophysical properties of Ca^{2+} channels, as well as potential consequences on synaptic functions. Our study identified a strongly reduced surface expression and presynaptic localization of mouse $\alpha_2\delta$-2 containing the p.R596P mutation, homologous to human p.R593P. Upon heterologous co-expression, this resulted in altered $Ca_V1.3$ current properties, whereas the current density of $Ca_V2.1$ was not affected. Nevertheless, homologous expression of p.R596P in hippocampal neurons affected the ability of $\alpha_2\delta$-2 to induce a statistically significant increase in the presynaptic abundance of endogenous $Ca_V2.1$ and, consequentially, Ca^{2+} transients. Most importantly, our study identified three consequences of the p.R596P mutation on synaptic functions: firstly, reduced, albeit still functional trans-synaptic coupling to postsynaptic receptors, secondly, reduced presynaptic synapsin clustering in glutamatergic nerve terminals, and thirdly, reduced amplitudes of glutamatergic miniature postsynaptic currents (mEPSCs). Taken together, our data strengthen the hypothesis that the human p.R593P mutation in $\alpha_2\delta$-2 is causal for the clinical symptoms of the siblings and demonstrate that disease-associated $\alpha_2\delta$ mutations can alter channel-dependent as well as synaptic functions of $\alpha_2\delta$ proteins, both of which may contribute to the pathophysiological mechanism.

2 | METHODS

2.1 | Animal and ethical approval

Animal procedures for wild-type BALB/c mice were performed at the Medical University Innsbruck in compliance with EU and national regulations. Original wild-type BALB/c mice for starting the breeding colony were bought from Charles River (Germany).

TABLE 1 Previously reported cases of infantile-onset epilepsy with bi-allelic mutations in CACNA2D2.

Publication	Genetic alteration	Patient	Common main symptoms	Seizure onset (month)	Functional characterization
Edvardson et al., 2013	Homozygous c.3199A > g (p.L1040P)	Three affected siblings (2 Female, 1 Male)	• Infantile-onset epilepsy • Global developmental Delay • Cerebellar atrophy	1–2	Failed to increase current density of both N ($Ca_V2.2$) and L ($Ca_V1.2$) Type Ca^{2+} channels when expressed in Xenopus oocytes
Pippucci et al., 2013	Homozygous c.1295delA (p.Asn432fs)	Male		5	Abolished $\alpha_2\delta-2$ protein expression in patient
Butler et al., 2018	Compound Heterozygous c.782C > T (p.Pro261Leu) c.3137T > C (p.Leu1046Pro)	Male		7	Not available
Punetha et al., 2019	Homozygous c.485_486del (p.Tyr162Ter)	Male		7	
	Homozygous c.1778G > C (p.Arg593Pro)	Two affected siblings (1 female, 1 male)		1–2	The present study

Note: Summary of the clinical and molecular features of individuals with rare biallelic CACNA2D2 variants (Butler et al., 2018; Edvardson et al., 2013; Pippucci et al., 2013; Punetha et al., 2019).

The animal facility of the Medical University of Innsbruck was approved as user by the Austrian Federal Ministry of Science, Research and Economy in accordance with §16 TVG 2012, license numbers BMWF-66.011/0017-II/3b/2014 and BMWF-66.011/0067-II/3b/2014. Mice were maintained in groups of 3–5 per cage at the central animal facility in Innsbruck under standard housing conditions with food and water available ad libitum on a 12 h light/dark cycle. Mice used for breeding were 2 to 14 months old. According to the RRR principle, the number of mice used was kept to the minimum necessary for a statistical representative analysis, which was comparable to numbers reported in previous studies. In total, 13 pregnant mice were used for hippocampal culture preparations. No ethics vote was required, and anonymized information about the patients was quoted from a published study (Punetha et al., 2019).

2.2 | Cell culture and transfection procedures

2.2.1 | Primary cultured hippocampal neurons

Low-density hippocampal cultures were generated from 16.5- to 18-day-old embryonic BALB/c mice of either sex as described previously (Geisler et al., 2019; Kaech & Banker, 2006; Obermair et al., 2004). Briefly, pregnant mice were killed by cervical dislocation, embryos were immediately extracted and decapitated. For each culture preparation, 2–8 hippocampi were dissected in cold Hank's balanced salt solution (HBSS, Gibco, cat. no. 14180-046), pooled, and dissociated by 2.5% trypsin (Gibco, cat. no. 15090-046) treatment and subsequent trituration. Dissociated neurons were plated at a density of ~3500 cells/cm^2 (immunolabeling experiments) or 7000 cells/cm^2 (whole-cell patch-clamp recordings), on five 18 mm glass coverslips (Marienfeld Superior, cat. no. 0111580) coated with poly-l-lysine (Sigma-Aldrich, cat. no. P2636) in neuronal plating medium [minimum essential medium (MEM, Gibco, cat. no. 41090-028), supplemented with 1 mM pyruvic acid (Sigma, cat. no. P2256), 0.6% glucose (Carl Roth, cat. no. HN06.3), and 10% horse serum (Gibco, cat. no. 16050-122)]. After attachment of neurons for 3–4 h, coverslips were transferred neuron-side down into a 60 mm culture dish containing a feeder monolayer of glia. Three days after plating, glial proliferation was inhibited with 5 µM Ara-C (Sigma, cat. no. C6645). Neurons and glia were maintained in NBKO [serum-free neurobasal medium (Gibco, cat. no. 21103-049) supplemented with Glutamax (Gibco, cat. no. 35050-038) and B-27 (Gibco, cat. no. 17504-044)] that was changed weekly by replacing one-third of the volume with fresh maintenance medium. On day in vitro (DIV) six, neurons were transfected with plasmids using Lipofectamine 2000 (Thermo Fisher Scientific, cat. no. 11668019) as described previously (Obermair et al., 2004). 1.5 µg of total DNA was used for co-transfections at equimolar ratios. For presynaptic Ca^{2+} measurements and whole-cell patch-clamp recordings, neurons were used between DIV14 and 17, whereas for immunolabeling experiments, neurons were processed between DIV21 and 25.

2.2.2 | tsA201 cells

Human embryonic kidney (HEK)-293 subclone stably expressing SV40 temperature-sensitive T antigen (tsA201) cells [ECACC cat. No. 96121229, RRID:CVCL_2737, not listed as a commonly misidentified cell line by the International Cell Line Authentication Committee (ICLAC; http://iclac.org/databases/cross-contaminations/)] was cultured in Dulbecco's modified Eagle's medium (DMEM; Gibco, cat. no. 11995065) completed with 10% FBS (Gibco, cat. no. 10270106), 0.1 U/mL penicillin, and 0.1 µg/mL

streptomycin (PenStrep, Gibco, cat. no. 15140-122), and were maintained at 37°C in a humidified incubator with 5% CO_2. Cells were split when they reached ~80% of confluence using 0.5% trypsin–EDTA (Gibco, cat. no. 15400-054) for detaching adherent cells. The cell's passage number did not exceed 20 passages. For whole-cell patch-clamp recordings, tsA201 cells were transiently transfected with α_1 and β subunit as a control condition or together with WT or mutated $\alpha_2\delta$-2 at equimolar ratios using FuGeneHD transfection reagent (Promega, cat. no. E2311) according to the manufacturer protocol. eGFP was always included as a marker for transfected cells. One day after transfection, cells were detached and replated at very low density on poly-l-lysine-coated 35 mm Petri dishes and kept at 30°C and 5% CO_2 to increase protein expression and inhibit cell proliferation. Cells were used for electrophysiology experiments 48–72 h after transfection. For live-cell Immunolabeling experiment, cells were plated on 13 mm glass coverslips (Marienfeld Superior, cat. no. 0111530) coated with poly-l-lysine. For western blot and live-cell immunolabeling experiments, tsA201 cells were transfected with 1 µg 2HA-tagged $\alpha_2\delta$-2 together with 0.5 µg eGFP. Experiments were performed 48 hours after transfection.

2.2.3 | Lentiviral production

Lentiviruses were produced by transient transfection of confluent Lenti-X 293T cells (Takara cat. no. 632180), with the lentiviral expression vectors containing pHR-βA-eGFP, pHR-βA-eGFP*$\alpha_2\delta$-2, or pHR-βA-eGFP*$\alpha_2\delta$-2_R596P together with psPAX2 (packaging plasmid) and pVSV (envelope plasmid) using Metafectene (Biontex Laboratories, cat. no. T020-1.0). The following day, sodium butyrate was added (5 mM final concentration) to cells early in the morning to enhance viral production. Six hours later, medium was changed to neuronal plating medium (NPM; consisting of MEM, 10% horse serum, 0.6% glucose, and 1 mM sodium pyruvate), and after 24 h, supernatants containing the viruses were harvested, sterile filtered (0.45 µm syringe filter, Sarstedt, cat. no. 83.1826), aliquoted, and stored at −20°C. Cultured hippocampal neurons were infected immediately after plating with the lentiviral medium supernatant diluted 1:2 in NPM with 3 µg/mL polybrene (Millipore Sigma, cat. no. TR-1003-G) and incubated for 4 h in a humidified incubator (5% CO_2) at 37°C.

2.3 | Expression vectors and cloning procedures

All plasmids used to transfect primary cultured hippocampal neurons were cloned into an eukaryotic expression plasmid containing a neuronal chicken β-actin promoter (pβA) to improve neuronal expression. All newly generated constructs were verified by Sanger sequencing (Eurofins Genomics or Microsynth). The cloning procedures to generate the following plasmids were described previously: pβA-$\alpha_2\delta$-2-v1 (Geisler et al., 2019), pβA-2HA-$\alpha_2\delta$-2-v1 (Geisler et al., 2019), pSyn-GCaMP6f (Brockhaus et al., 2019), pβA-$\alpha_2\delta$-2-ΔMIDAS (Schopf et al., 2021), pHR-pβA-eGFP*$\alpha_2\delta$-2-v1 (Geisler et al., 2019), pβA-eGFP (Obermair et al., 2004), pHR-pβA-mCherry (Geisler et al., 2019), pGFP$^-$-$Ca_V1.3$ (Koschak et al., 2001), pCMV-$Ca_V2.1$ (Mullner et al., 2004), β3 (Castellano et al., 1993), and β4 (Etemad et al., 2014).

pβA-$\alpha_2\delta$-2-v1_R596P: The p.R596P mutation was introduced by PCR with mutagenesis primers with overlapping extensions. Briefly, $\alpha_2\delta$-2-v1 cDNA sequence was amplified with mutagenesis primers having 21 overlapping bases in two separate PCR reactions using pβA-$\alpha_2\delta$-2-v1 as template (mouse $\alpha_2\delta$-2-v1 cDNA, GenBank accession number MK327277). For the first PCR reaction, the forward mutagenic primer sequence was 5′-gaggagatccctcgcagcatgattgacggc-3′ and the reverse primer sequence was 5′-gacgacctagactgagctcc-3′. For the second PCR reaction, the forward primer sequence was 5′-gacgctgcagagaatttcca-3′ and the reverse mutagenic primer sequence was 5′- catgctgcgaggatctcctccttgttctc-3′. The two separate PCR products were then used as templates for a final PCR reaction with the two flanking primers to connect the nucleotide sequences. The resulting fragment was then EcoRI/BglII digested and ligated into the corresponding site of pβA-$\alpha_2\delta$-2-v1 yielding pβA-$\alpha_2\delta$-2-v1_R596P.

pβA-2HA-$\alpha_2\delta$-2-v1_R596P: pβA-$\alpha_2\delta$-2-v1_R596P was EcoRI/BglII digested and the fragment containing the p.R596P mutation was ligated into the corresponding site of pβA-2HA-$\alpha_2\delta$-2-v1 (mouse $\alpha_2\delta$-2-v1 cDNA sequence with a double hemagglutinin (2HA) tag at the N-terminus after the predicted signal peptide cleavage site) yielding pβA-2HA-$\alpha_2\delta$-2-v1_R596P.

pHR-pβA-eGFP$\alpha_2\delta$-2-v1_R596P*: pβA-$\alpha_2\delta$-2-v1_R596P was NheI/RsrII digested and the fragment containing the p.R596P mutation was ligated into the corresponding site of pHR-pβA-eGFP*$\alpha_2\delta$-2-v1 yielding pHR-pβA-eGFP*$\alpha_2\delta$-2-v1_R596P.

2.4 | Immunocytochemistry and high-resolution fluorescence microscopy

Permeabilized or live-cell immunolabeling of neurons was performed as described previously (Folci et al., 2018; Geisler et al., 2019; Obermair et al., 2004; Schopf et al., 2021; Stanika et al., 2016), and information on primary and secondary antibodies is summarized in Table 2. For permeabilized staining, neurons were fixed with 4% paraformaldehyde and 4% sucrose in PBS (pF) for 20 min at room temperature, washed, and incubated for 30 min in 5% normal goat serum in PBS-containing 0.2% bovine serum albumin (BSA) and 0.2% Triton X-100 (PBS/BSA/Triton) to enable membrane permeabilization. Primary antibodies (Table 2) diluted in PBS/BSA/Triton were applied overnight at 4°C and detected by fluorochrome-conjugated Alexa secondary antibodies incubated for 1 h at room temperature. For live-cell surface staining of HA-tagged $\alpha_2\delta$ proteins, transfected neurons were incubated with rat-anti-HA antibody diluted in glia-conditioned neurobasal medium for 10 min at 37°C following quick rinsing in warm HBSS and fixation with pF for 10 min at room temperature. Subsequent washing and blocking steps as well as 1 h incubation with fluorochrome-conjugated secondary goat anti-rat

TABLE 2 List of antibodies used in this study.

Antibody	Species	Dilution	Source
Anti-HA	Rat, clone 3F10	1:100 (Live/A594)	Roche (cat. no. 11867423001, RRID:AB_390918)
Anti-HA	Mouse, clone 5B1D10	1:1000 (WB)	Thermo Fisher Scientific (cat. no. 32–6700, RRID:AB_2533092)
Anti-$GABA_AR_{\beta 2/3}$	Mouse, clone bd17	1:500 (A594)	Millipore (cat. no. MAB341, RRID:AB_2109419)
Anti-synapsin1	Mouse, clone 46.1	1:500 (A350)	Synaptic Systems (cat. no. 106011, RRID:AB_2619772)
Anti-vGLUT1	Rabbit, polyclonal	1:2000 (A350)	Synaptic Systems (cat. no. 135002, RRID:AB_2315546)
Anti-$Ca_V2.1$	Rabbit, polyclonal	1:2000 (A594)	Synaptic Systems (cat. no. 152203, RRID:AB_2619841)
Anti-GAPDH	Mouse, clone 6C5	1:10000	Santa Cruz Biotechnology (cat. no. sc-32 233, PRID:AB_627679)
Alexa Fluor 350	Goat anti-rabbit	1:500	Thermo Fisher Scientific (cat. no. A-21068, RRID:AB_2535729)
	Goat anti-mouse	1:500	Thermo Fisher Scientific (cat. no. A-21049, RRID:AB_2535717)
Alexa Fluor 594	Goat anti-rabbit	1:4000	Thermo Fisher Scientific (cat. no. A-11037, RRID:AB_2534095)
	Goat anti-mouse	1:4000	Thermo Fisher Scientific (catalog #A-11032, RRID:AB_2534091)
	Goat anti-rat	1:4000	Thermo Fisher Scientific (catalog #A-11007, RRID:AB_10561522)
Secondary antibody coupled to HRP	Goat anti-mouse IgG [H + L]	1:20000	Thermo Fisher Scientific (catalog #G21040, RRID:AB_2536527)

Note: Summary of primary and secondary antibodies used in immunocytochemistry and western blot.

Alexa Fluor 594 antibody were conducted with PBS and PBS/BSA, respectively. After washing and fixing cells in pF for 5 min, neurons were permeabilized by blocking solution (PBS/BSA/Triton) and incubated with primary mouse-anti-synapsin antibody overnight at 4°C and detected with goat-anti-mouse Alexa Fluor 350 antibody. Coverslips were mounted on microscopy slides neuron-side down in DABCO glycerol solution (Carl Roth, cat. no. 0718.1) to retard photobleaching. Hippocampal neurons were imaged with a BX53 microscope (Olympus) using a 60 X 1.42 numerical aperture (NA) oil immersion objective lens. Fourteen-bit grayscale images were recorded with a cooled CCD camera (XM10; Olympus) using cellSens Dimension software (Olympus) and further analyzed in MetaMorph software (Molecular Devices). To analyze presynaptic and postsynaptic protein composition, images of randomly selected well-differentiated and positively transfected cells were acquired with the same exposure and gain settings for all conditions within an experiment. Only cells with medium eGFP expression were selected for the analysis, and overly saturated neurons (based on eGFP levels) were excluded from analysis. Figures were assembled in Adobe Photoshop CS6 using linear adjustments to correct black level and contrast.

2.5 | Antibodies

Information on primary and secondary antibodies used in this study is summarized in Table 2.

2.6 | Image analysis and quantification

2.6.1 | Colocalization of synaptic proteins

To visualize the synaptic localization of HA-tagged $\alpha_2\delta$ subunits, as well as presynaptic (synapsin, vGLUT1, $Ca_V2.1$) and postsynaptic proteins ($GABA_AR$) of representative images (Figures 6, 7 and 9), lines were manually placed across the single-/double-/triple-labeled synapses and intensities were recorded using the "line scan" function of MetaMorph (Molecular Devices) (Di Biase et al., 2009). Average fluorescence intensities of respective signals were measured along a 3 µm length line, followed by background subtraction, and plotted in Microsoft Excel.

2.6.2 | Quantification of fluorescent clusters in single boutons

To analyze the effects of homologous presynaptic expression of WT or mutated $\alpha_2\delta$-2 subunit on synapse composition of cultured hippocampal neurons, images from triple-fluorescence labeling were acquired from the eGFP (green), $GABA_AR_{\beta 2/3}$ (red), and vGLUT1 (blue) channels. Images were analyzed with a custom-programmed and semi-automated MetaMorph journal (Molecular Devices), as described previously (Geisler et al., 2019; Schopf et al., 2021). Briefly, corresponding eGFP and vGLUT1 images were superimposed, eGFP/vGLUT1-positive varicosities (putative glutamatergic synapses) were randomly chosen as regions of interest (ROIs), and a background region was selected for background subtraction. Axonal varicosities were defined as prominent swellings with higher fluorescence signals compared to the adjacent axonal shaft. Subsequently, $GABA_AR$ and vGLUT1 grayscale images were measured without thresholding to avoid potential cut-off of the fluorescent signal. By applying the "shrink region to fit" tool, automatic boundaries were drawn according to the threshold enabling only colocalized clusters to be analyzed, and selected ROIs were then transferred from the eGFP image to the $GABA_AR$ and vGLUT1 images to measure fluorescent intensities. For the individual synapses in each of the channels, the following parameters were detected in a blinded manner: eGFP threshold area as a measure for bouton size and average and integrated fluorescence intensities providing information on the

size and intensity of clusters. In the same manner, the quantification of $Ca_V2.1$ together with synapsin signals was performed.

2.6.3 | Quantification of live cell surface expression

To analyze presynaptic targeting of HA-tagged $\alpha_2\delta$, a slightly modified protocol was used because this staining pattern was not directly co-localizing with the corresponding presynaptic eGFP signal. Therefore, the presynaptic ROI was dilated by 0.5 µm, in order to avoid false-positive or false-negative staining patterns, as described in Schopf et al. (2021). The fluorescent intensity of live-cell-stained HA-tagged $\alpha_2\delta$ in the main three compartments of neurons was determined by measuring the fluorescent intensity along an outlined axon, dendrite, and cell soma.

2.6.4 | Quantification analysis

Analyses of all experiments were conducted with Microsoft Excel. For each neuron, an average fluorescence value from minimum of 10 presynaptic varicosities was calculated and plotted in GraphPad Prism 8. For each condition, minimum of 30 cells were considered from three to four independent culture preparations. All values were additionally normalized to the control condition.

2.7 | Calcium imaging

To examine presynaptic Ca^{2+} influx, GCaMP6f coupled to synaptophysin driven by a synapsin promotor (Brockhaus et al., 2019) was used to conduct Ca^{2+} imaging as described previously (Ablinger et al., 2022). Briefly, primary neurons were transfected at DIV6 with pβA-SynGCaMP6f and pβA-mCherry, as a control condition, or together with WT or mutated $\alpha_2\delta$-2 subunit. Then, at DIV14-17, coverslips were mounted in a recording chamber, placed on an inverted microscope (Olympus IX71, 60×, 1.42 NA PlanApo objective), and superfused at 1.0–1.5 mL/min rate with bath solution (32°C), containing (in mM): 145 NaCl, 3 KCl, 1.5 $MgCl_2$, 2 $CaCl_2$, 11 glucose, and 10 HEPES. To suppress postsynaptic signaling, the following blockers were added to the bath solution (in µM): 10 6-cyano-7-nitroquinoxaline-2,3-dione (CNQX, Tocris, cat. no. 1045), 25 DL-2-amino-5-phosphonovaleric acid (DL-AP5, Tocris, cat. no. 3693), and 10 bicuculline (Tocris, cat. no. 0109); pH 7.3 adjusted with NaOH. A custom-built stimulation electrode was positioned with a micromanipulator (MPC-200, Sutter Instrument) and neurons were stimulated with 50 Hz trains of 1 and 10 current pulses (1 ms, 55 mA) as previously described (Ablinger et al., 2022; Schopf et al., 2021). Ca^{2+} transients were visualized and recorded (20 ms exposure time, frame rate 50 Hz, 200 frames, binning 2, and pixel size: 0.215 µm per pixel) with a CMOS camera (Orca Flash4.0, Hamamatsu), using a halogen lamp light source (HXP 120) in the green channel (excitation: 470/40 nm, emission: 525/50 nm). Recordings were controlled by Micromanager software (Vale Lab, UCSF). As a standard reference, 50 frames were recorded before the stimulus train was triggered and used to calculate the fluorescent baseline and to analyze differences in GCaMP6f presynaptic expression among experimental conditions.

2.7.1 | Data analysis

Recordings were analyzed with FIJI/ImageJ software (National Institute of Health) as described previously (Ablinger et al., 2022). Twenty regions of interest (ROIs) per recorded cell were drawn around active presynaptic boutons using the plugin "Time Series Analyzer V3" with an AutoROI diameter of 10 pixels and the "Subtract Background" tool of ImageJ (employing a "rolling ball" algorithm with a radius of 20 pixels ≈ 4.3 µm) was used to remove the background signal. The mean of the four highest fluorescence pixels was calculated for each ROI at each frame by applying a custom-made macro (Brockhaus et al., 2019) and further analysis was done in Microsoft Excel. To obtain mean sample traces, the changes in fluorescence as ΔF/F0 were calculated for each ROI, and 20 synapses per cell were averaged. The peak fluorescence amplitude for each ROI was obtained by averaging ΔF/F0 values from five frames after the pulse onset. Statistical analysis was performed on the mean peak amplitude of cells in GraphPad Prism 8.

2.8 | Electrophysiology

2.8.1 | tsA201 cells

$Ca_V2.1$ and $Ca_V1.3$ currents were measured using the whole-cell patch-clamp technique in voltage-clamp mode. Borosilicate glass capillaries (Sutter Instrument, model: BF150-75-10) were pulled with a micropipette puller (P-97, Sutter Instrument) and fire polished using a MF-830 microforge (Narishige Co). Patch pipettes had a resistance of 2–3.5 MΩ when filled with internal solution containing (in mM): 135 cesium chloride (CsCl, Sigma, cat. no. C3309), 10 Cs-EGTA (Carl Roth, cat. no. 3054.2), 1 magnesium chloride ($MgCl_2$, Sigma, cat. no. M0250), 10 HEPES (Carl Roth, cat. no. 6763.1), and 4 Na_2ATP (Sigma, cat. no. A1852-1VL) adjusted to pH 7.3 with 1 M cesium hydroxide (CsOH, Sigma, cat. no. 232068). For measuring Ca^{2+} current of $Ca_V1.3$, bath solution with 15 mM Ca^{2+} was used, containing (in mM): 15 calcium chloride ($CaCl_2$, Carl Roth, cat. no. 5239.2), 150 Choline-Cl (Sigma, cat. no. C1879), 1 $MgCl_2$, and 10 HEPES, adjusted to pH 7.3 with 1 M CsOH. For measuring Ca^{2+}, current through $Ca_V2.1$ bath solution with 2 mM Ca^{2+} was used containing (in mM): 2 $CaCl_2$, 170 Choline-Cl, 1 $MgCl_2$, 10 HEPES, adjusted to pH 7.3 with 1 M CsOH. Whole-cell patch-clamp recordings were performed at room temperature (20–23°C) using an EPC 10 amplifier controlled by Patch Master Software (HEKA Elektronik). Linear leak and capacitive currents were digitally subtracted with a P/4online protocol. Current–voltage (I-V) relationships were measured by applying 50 ms depolarizing square pulses to various test potentials (from −80 mV to +90 mV) in steps of

5 mV, and holding potential (HP) was set to −80 mV. I-V curves were fitted according to a Boltzmann equation:

$$I = G_{MAX} \times (V - V_{rev}) / \left(1 + e^{-(V-V_{0.5})/k}\right)$$

where I is the peak current, G_{MAX} is the maximum conductance, V is the test potential, V_{rev} is the extrapolated reversal potential, $V_{0.5}$ is the half-maximal activation voltage, and k is the slope factor. The voltage dependence of activation was obtained from the I–V relationship by calculating the conductance $G = I / (V_{rev} - V)$ followed by normalization (G / G_{MAX}) and plotting as a function of voltage. The G-V curve was fitted using the following Boltzmann relationship:

$$G = G_{MAX} / \left(1 + e^{-(V-V_{0.5})/k}\right)$$

Series resistance was compensated by 80%–95% and recordings were accepted for analysis when the I_{peak} was greater than 100 pA and smaller than 3 nA in size. Voltages were not corrected for the liquid junction potential (−9 mV).

2.8.2 | Primary cultured hippocampal neurons

Spontaneous miniature excitatory postsynaptic currents (mEPSCs) of primary cultured hippocampal neurons were recorded at DIV 14 and 15 using the whole-cell patch-clamp technique at a holding potential of −70 mV as described previously (Schopf et al., 2021). Patch pipettes were pulled from Borosilicate glass capillaries (Sutter Instrument, model: BF150-75-10), fire polished, and had resistances of 2.5–4 MΩ when filled with the following internal solution (in mM): 130 Cs-methane sulfonate, 10 CsCl, 1 $MgCl_2$, 0.1 $CaCl_2$, 10 HEPES, 2 EGTA, 4 Mg-ATP (Sigma, cat. no. G8877), and 0.3 Na-GTP (Sigma, cat. no. A9187), pH 7.2 with KOH (Carl Roth, cat. no. 6751.1). The bath solution contained the following (in mM): 137 sodium chloride (NaCl, Carl Roth, cat. no. 3957.1), 3 potassium chloride (KCl, Carl Roth, cat. no. 6781.3), 10 HEPES, 2 $MgCl_2$, 1.8 $CaCl_2$, 10 glucose, 0.05 DL-AP5, 0.05 bicuculline, and 0.001 tetrodotoxin (TTX, Tocris, cat. no. 1078) pH 7.4 with NaOH. Currents were recorded with an EPC 10 amplifier, controlled by PatchMaster software (HEKA Elektronik Dr. Schulze GmbH, Germany), and analyzed using Mini analysis software (Symaptosoft, USA). Frequency and average amplitude of mEPSC of each cell were normalized to the corresponding mean value of the control condition for each experiment separately.

2.9 | Western blotting

To determine total protein levels of WT and mutated $\alpha_2\delta$-2, whole-cell lysates (WCL) from tsA201 cells transfected with 2HA-tagged $\alpha_2\delta$-2 were prepared and immunoblotted. At 48 h after transfection, cells were rinsed with phosphate-buffered saline (PBS) harvested and resuspended in 200 µL ice-cold RIPA buffer containing: 50 mM Tris–HCl pH 8.0, 150 mM NaCl, 0.1% SDS, 10 mM NaF, 0.5 mM EDTA, 10% Glycerol, and 1% Igepal, supplemented with protease inhibitor cocktail (Thermo Scientific, cat. no. 87785) and lysed on ice for 30 min. Lysates were then cleared by centrifugation at 13000×g for 15 min and assayed for total protein concentration using Pierce BCA protein assay kit (Thermo Scientific, cat. no. 23227). Fifty microgram of proteins were then resuspended in NuPAGE™ LDS Sample Buffer (Invitrogen, cat. no. NP0008), with 50 mM dithiothreitol (DTT, Invitrogen, cat. no. NP0004), and separated on precast gradient polyacrylamide gels (NuPAGE™ 4 to 12%, Bis-Tris, Thermo Scientific, cat. no. NP0336BOX) and transferred to polyvinylidene fluoride (PVDF) membranes with 0.45 µm pore size (Immobilon, cat. no. IPVH00010). Membranes were blocked with 5% milk in Tris-buffered saline (10 mM Tris-Base and 0.85% NaCl) with 0.3% Tween (TBS-T) for 30 min at RT, followed by incubation with the indicated primary antibody overnight at 4°C. The following day membranes were washed three times with TBS-T and incubated with secondary antibodies coupled to HRP for 60 min and washed three times for 10 min with TBST-T. The signal was obtained by HRP reaction with SuperSignal™ West Pico PLUS Chemiluminescent Substrate (Thermo Scientific, cat. no. 34580) and membranes were scanned for protein detection with an Intas NEW-Line ECL ChemoStar Touch Imager HR 9.0 (for HRP) and subsequent protein quantification was performed with Image Studio Light and Microsoft Excel. The signal intensity of 2HA-$\alpha_2\delta$-2 was normalized to the signal intensity of the loading internal control GAPDH. Then, the relative signal intensities were normalized to the corresponding WT 2HA-$\alpha_2\delta$-2 relative signal intensity for each experiment separately.

2.10 | Homology modeling

The structural homology model of mouse $\alpha_2\delta$-2 protein was obtained by superposing the predicted AlphaFold human $\alpha_2\delta$-2 (Jumper et al., 2021; Varadi et al., 2022) onto the published cryo-EM structure of human $\alpha_2\delta$-1 subunit within the $Ca_V2.2$ complex (PDB code: 7MIY) using PyMOL (The PyMOL Molecular Graphics System, Version 2.3.2. Schrödinger, LLC, New York, NY, USA). PyMOL was used to prepare the figure.

2.11 | Experimental design and statistical analysis

Number of mice used in this study was kept to the minimum necessary for a statistical representative analysis, according to the RRR principle. Where possible, investigators were blinded during experiments and analyses. Three to four independent hippocampal culture preparations were analyzed per experiment and details on cell or bouton numbers are given in the respective figure legends. Electrophysiological recordings in tsA201 cells were obtained from three to four independent experiments (i.e., cell passage and transfection). Details on cell, bouton, or recording numbers are given in the respective figure legends. The distribution of all acquired data was visually assessed using the frequency distribution function of GraphPadPrism 9. In cases where a systematic influence (e.g., tendency to values approaching

0) prevented a normal distribution (e.g., calcium imaging, surface expression analysis in tsA201 cells), statistical analyses were performed on log-transformed data. All data are shown as mean ± SEM. No test for outliers was conducted and all data points were included in the analysis. Significance levels (*p*-values) of statistical tests and post hoc analysis are presented in the respective figure legends. The model in Figure 1 was generated with PyMOL (The PyMOL Molecular Graphics System, Version 2.3.2.). Data, graphs, and figures were organized, analyzed, and assembled using MicrosoftExcel, GraphPadPrism 6, SigmaPlot (Systat Software), Adobe PhotoshopCS6, and Affinity Photo. Data contained within the article, and raw data presented in this study are available upon request.

3 | RESULTS

3.1 | The evolutionarily conserved arginine 596 (R596) is predicted to be critical for the protein structure of $\alpha_2\delta$-2

Amino acid sequence alignment of $\alpha_2\delta$-2 from different species shows that human arginine 593 (R593) is an evolutionary conserved amino acid (Figure 1a). Human R593 corresponds to mouse R596 and because we used mouse cDNA in our studies, the residue numbering hereafter refers to mouse $\alpha_2\delta$-2. $\alpha_2\delta$-2 is post-translationally cleaved into α_2 and δ peptides that are linked to each other by disulfide bonds and R596 is located within the α_2 peptide (Figure 1b). Structural homology modeling predicts an interaction of R596 with tyrosine 1094 (Y1094) within the δ peptide (Figure 1c), suggesting an important role of R596 in maintaining and stabilizing the interaction between the two peptides. Therefore, we hypothesize that R593 is critical for the structural integrity of $\alpha_2\delta$-2 and that mutations at this position may alter protein functions.

3.2 | Reduced membrane expression of epitope-tagged $\alpha_2\delta$-2_R596P upon heterologous expression in tsA201 cells

To study the consequences of the human p.R593P mutation on the protein membrane expression, we introduced the corresponding mutation into the mouse-coding sequence of $\alpha_2\delta$-2 (p.R596P). HA epitope-tagged wild-type (WT) or mutated $\alpha_2\delta$-2 were expressed together with soluble eGFP in tsA201 cells. Anti-HA live-cell labeling of WT $\alpha_2\delta$-2 revealed a striking membrane expression identified by a fine-dotted pattern along the surface of tsA201 cells (Figure 2a,

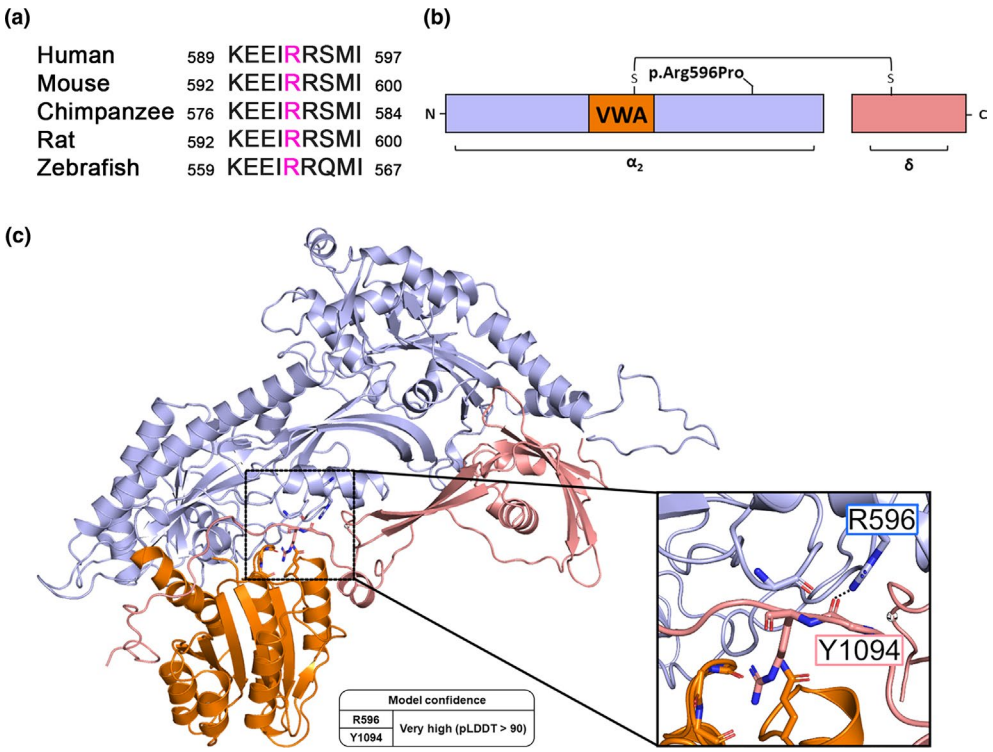

FIGURE 1 The conserved R596 residue is predicted to have a critical role in stabilizing the interaction between α_2 and δ peptides. (a) Sequence alignment between $\alpha_2\delta$-2 proteins from different species. Position corresponding to human arginine 593 (R596 in mouse $\alpha_2\delta$-2) is highlighted in purple. (b) Schematic overview of $\alpha_2\delta$-2 protein illustrating the positions of the von Willebrand factor type A domain (VWA) and the p.R596P mutation. (c) Structural homology modeling of mouse $\alpha_2\delta$-2 protein based on the published Cryo-EM structure of the human $Ca_V2.2$ channel complex (PDB code: 7MIY) predicts a critical interaction of the side chain of R596 (α_2 peptide) with the backbone of Y1094 residue (δ peptide) through a hydrogen bond. (Color code: α_2 peptide in purple, VWA domain in orange, and δ peptide in pink.) AlphaFold per-residue model confidence scores (pLDDT) for R596 and Y1094 residues are very high (97.38 and 94.25, respectively).

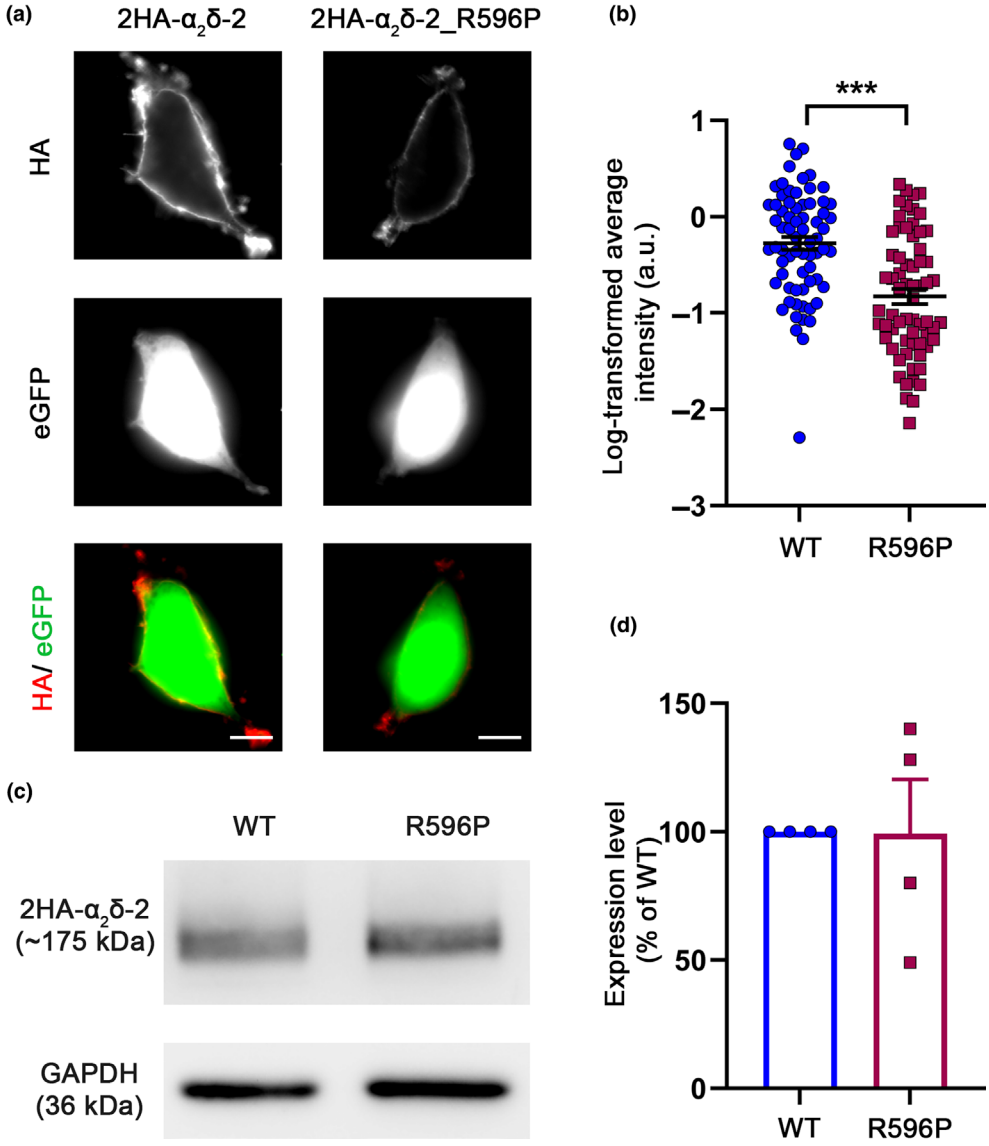

FIGURE 2 Reduced membrane expression of $\alpha_2\delta$-2_R596P compared to WT $\alpha_2\delta$-2 in tsA201 cells. tsA201 cells were transfected with soluble eGFP together with either HA-tagged WT or mutated $\alpha_2\delta$-2 (R596P) and were live-cell labeled with an antibody against the HA epitope. (**a**) Representative images of anti-HA live-cell-labeled tsA201 cells transfected with 2HA-$\alpha_2\delta$-2 or 2HA-$\alpha_2\delta$-2_R596P. Membrane expression of HA-tagged WT $\alpha_2\delta$-2 is identified by a fine-dotted pattern along the surface of tsA201 cells. In contrast, dots of 2HA-$\alpha_2\delta$-2_R596P labeling are sparsely localized on the cell surface, and overall fluorescence intensity is lower. (**b**) Quantification of $\alpha_2\delta$-2 surface expression. Log-transformed anti-HA live-cell-staining intensities (arbitrary units) are shown for individual cells (dots) and means ± SEM (lines). Data were obtained from three independent experiments and 69 and 66 cells transfected with WT or mutated HA-tagged $\alpha_2\delta$-2 were analyzed, respectively. (**c**) Immunoblot of whole-cell lysates obtained from tsA201 cells transfected with 2HA-tagged WT or mutated $\alpha_2\delta$-2. $\alpha_2\delta$-2 protein was detected with an anti-HA antibody (upper panel), and anti-GAPDH labeling was used as loading control (lower panel). (**d**) Quantification of the total protein expression levels of WT and mutated $\alpha_2\delta$-2. Relative total protein expression levels of 2HA-tagged $\alpha_2\delta$-2_R596P were normalized to WT 2HA-tagged $\alpha_2\delta$-2 expression levels for each individual experiment (culture preparation). Data were obtained from four independent cell transfections, and values of individual experiments (dots) and mean bars ± SEM (lines) are shown. **Statistics**: (b) unpaired two-tailed t-test, $t_{(133)} = 5.4$; $^{***}p < 0.0001$; (d) unpaired two-tailed t-test performed on raw data, $t_{(6)} = 0.42$; $p = 0.69$. Scale bars, 10 μm.

left panel). In comparison to WT $\alpha_2\delta$-2, surface expression of the mutated $\alpha_2\delta$-2_R596P was strongly reduced (Figure 2a,b). Generally, the p.R596P mutation may impair protein folding resulting in accelerated protein degradation. To test this hypothesis, we performed western blot analysis of whole-cell lysates from tsA201 cells transfected with WT or mutated HA-tagged $\alpha_2\delta$-2. Overall, $\alpha_2\delta$-2 protein levels were comparable between tsA201 cells transfected with WT or mutated proteins, showing that the p.R596P mutation does not alter protein expression levels (Figure 2c,d). Taken together, these data show a strongly reduced membrane expression of HA-tagged $\alpha_2\delta$-2_R596P compared to WT $\alpha_2\delta$-2, which is not caused by an altered protein expression level.

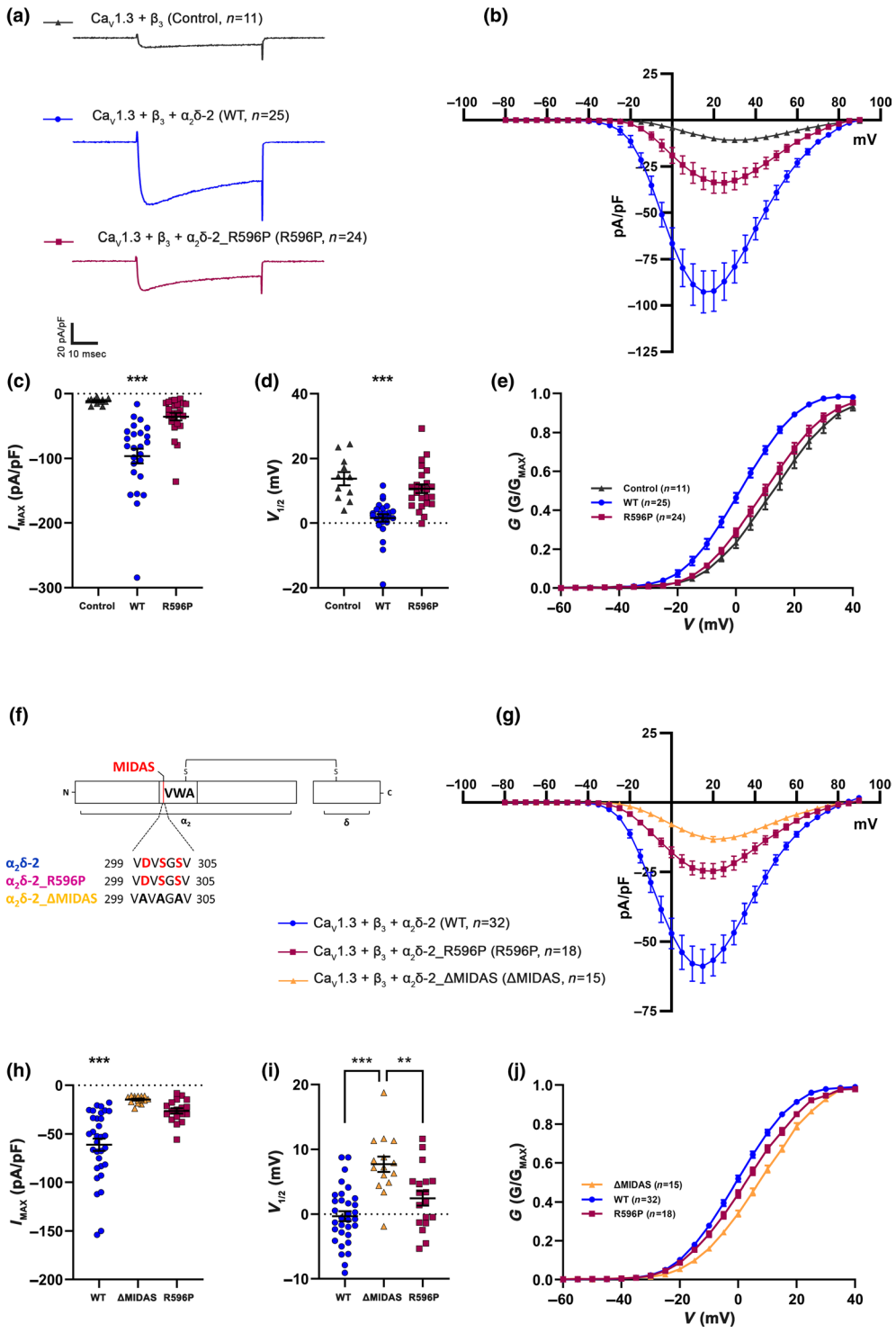

3.3 | The p.R596P mutation alters calcium current properties of the L-type channel $Ca_V1.3$

Various heterologous co-expression studies revealed that $\alpha_2\delta$ subunits increase the current density of Ca_V1 and Ca_V2 channels when expressed in combination with a β subunit (reviewed in Davies et al., 2007; Dolphin, 2016). Because the single-channel conductance was not altered by $\alpha_2\delta$ subunits (Barclay et al., 2001; Brodbeck et al., 2002), the proposed mechanism underlying the increase in current density is an increase in the number of functionally expressed channels. In addition to the increase in current density, $\alpha_2\delta$ proteins have been shown to modulate the kinetics and voltage-dependent properties of Ca^{2+} currents depending on the α_1 subunit isoform (Obermair et al., 2005; Tuluc et al., 2007). Hence, we next analyzed whether and how the p.R596P mutant with its strongly reduced membrane expression affects the channel-dependent functions of $\alpha_2\delta$-2. Because $\alpha_2\delta$-2 is predominantly expressed in cerebellar Purkinje cells and inner hair cells of

FIGURE 3 p.R596P reduces current density and alters voltage dependence of activation of the L-type Ca^{2+} channel $Ca_V1.3$. (a–e) Ca^{2+} current properties of $Ca_V1.3$ channels recorded from tsA201 cells transfected with $Ca_V1.3$ and β_3 alone (control, gray triangles) or together with wild-type (WT, blue circles) or mutated $\alpha_2\delta$-2 (R596P, pink rectangles). Fifty msec test pulses from a holding potential of −80 mV to +90 mV were applied in 5 mV increments. Representative whole-cell Ca^{2+} current traces at V_{MAX} (a), current–voltage relationships (b), peak current densities (c), and half-maximal activation potentials (d) of the respective experimental conditions. (e) Fractional activation of the total $Ca_V1.3$ channel populations of the respective experimental conditions. **Statistics**: One-way ANOVA with Tukey's multiple-comparison test was performed on 11–25 recordings per condition; (c) maximal current density: $F_{(2,57)} = 21.3$; $p < 0.0001$. *P*-values of the post hoc test for the respective pairwise comparisons: $P < 0.0001$ for control versus WT, $p = 0.26$ for control versus R596P, and $p < 0.0001$ for WT versus R596P. (d) Half-maximal activation potential: $F_{(2,57)} = 19.1$; $p < 0.0001$. *P*-values of the post hoc test for the respective pairwise comparisons: $P < 0.0001$ for control versus WT, $p = 0.38$ for control versus R596P, and $p < 0.0001$ for WT versus R596P. Recordings were obtained from three independent experiments. (f) Schematic representation of the different $\alpha_2\delta$-2 constructs used in this experiment. The MIDAS motif (highlighted in red) in the $\alpha_2\delta$-2_ΔMIDAS construct is mutated to alanines. (g–j) Current properties of $Ca_V1.3$ channels recorded from tsA201 cells co-transfected with $Ca_V1.3$ and β_3 together with $\alpha_2\delta$-2_ΔMIDAS (ΔMIDAS, orange triangles), wild-type $\alpha_2\delta$-2 (WT, blue circles), and $\alpha_2\delta$-2_R596P (R596P, pink rectangles). Current–voltage relationships (g), peak current densities (h), and half-maximal activation potentials (i) of the respective experimental conditions. (j) Fractional activation of the total $Ca_V1.3$ channel population of the respective experimental conditions. **Statistics**: One-way ANOVA with Tukey's multiple-comparison test was performed on 15–32 recordings per condition. (h) Maximal current density: $F_{(2,62)} = 20.1$; $p < 0.0001$. *P*-values of the post hoc test for the respective pairwise comparisons: $P < 0.0001$ for ΔMIDAS versus WT, $p = 0.40$ for ΔMIDAS versus R596P, and $p < 0.0001$ for WT versus R596P. (i) Half-maximal activation potential: $F_{(2,62)} = 15.8$; $p < 0.0001$. *P*-values of the post hoc test for the respective pairwise comparisons: $P < 0.0001$ for ΔMIDAS versus WT, $p = 0.005$ for ΔMIDAS versus R596P, and $p = 0.10$ for WT versus R596P. Recordings were obtained from four independent experiments. Significances of post hoc tests between conditions are indicated in the graphs by asterisks (***$p < 0.001$, **$p < 0.01$).

TABLE 3 Current properties of $Ca_V1.3$ in tsA201 cells.

	$Ca_V1.3/\beta_3$			$Ca_V1.3/\beta_3$		
	Control	WT	R596P	ΔMIDAS	WT	R596P
Current density (pA/pF)	−11.7 ± 1.5	−96.2 ± 11.3	−35.5 ± 5.8	−14.3 ± 1.0	−61.0 ± 6.3	−26.2 ± 2.7
$V_{1/2}$ (mV)	13.7 ± 2.0	1.5 ± 1.1	10.6 ± 1.3	7.7 ± 1.1	−0.3 ± 0.7	2.4 ± 1.1
V_{rev} (mV)	80.0 ± 1.4	70.3 ± 0.8	75.8 ± 1.0	71.1 ± 1.5	66.7 ± 0.6	68.2 ± 0.8
n	11	25	24	15	32	18

Note: All values are presented as mean ± SEM and were obtained from >3 independent experiments. $V_{1/2}$ and V_{rev} parameters were obtained by fitting the *I–V* curves to a Boltzmann function. $V_{1/2}$, Half-maximal activation potential; V_{rev}, extrapolated reversal potential; and *n*, number of recordings. For statistics, see Figure 3.

the cochlea, we focused on the most likely Ca_V subunit partners of $\alpha_2\delta$-2 in these cells, $Ca_V2.1$ (cerebellum) and $Ca_V1.3$ (inner hair cells) (Fell et al., 2016; Schlick et al., 2010). Moreover, these two Ca_V channel isoforms have a distinct subcellular distribution in neurons of the CNS. While $Ca_V1.3$ channels are predominantly localized at postsynaptic sites (Stanika et al., 2016), $Ca_V2.1$ channels are located at presynaptic terminals (Etemad et al., 2014). Hence, studying the consequences of the p.R596P mutation on these Ca_V channel isoforms provides insight into the involvement of pre- and postsynaptic compartments in the pathophysiology of p.R596P variant. We first studied the current properties of the L-type channel $Ca_V1.3$ by performing whole-cell patch-clamp recordings in tsA201 cells transfected with $Ca_V1.3$ and β_3 without (control) or together with WT or mutated $\alpha_2\delta$-2. As previously reported, the presence of $\alpha_2\delta$-2 significantly increased $Ca_V1.3$ current amplitudes and left shifted the voltage dependence of activation (Figure 3a–e). More importantly, co-expression of $\alpha_2\delta$-2_R596P failed to increase the current density of $Ca_V1.3$ to WT levels and prevented the left shift in the current–voltage relationship (Figure 3d; Table 3).

In theory, two mechanisms can contribute to the observed reduction in current density obtained when $\alpha_2\delta$-2_R596P was co-expressed with $Ca_V1.3$. Firstly, the p.R596P mutant may fail to support membrane trafficking of the channel complex. Secondly, the right shift in the current–voltage relationship may reduce the driving force at more positive potential, which is a known mechanism of $\alpha_2\delta$ protein action on L-type calcium channels (Obermair et al., 2008; Tuluc et al., 2007). Similar half-maximal activation potential obtained for cells expressing $\alpha_2\delta$-2_R596P or no $\alpha_2\delta$ (control) supports a failure in membrane trafficking. Hence, to test if $Ca_V1.3$ channels are still partly modulated by $\alpha_2\delta$-2_R596P, we compared the current properties with $Ca_V1.3$ channels co-expressed with an $\alpha_2\delta$-2_ΔMIDAS (DxSxS motif is mutated to alanines) deletion construct. The metal ion-dependent adhesion site (MIDAS) within the VWA domain of $\alpha_2\delta$-1 and $\alpha_2\delta$-2 has been previously shown to play a key role in channel trafficking. More precisely, mutating the MIDAS motif results in ER retention of $\alpha_2\delta$ proteins and thereby completely abolishes their ability to enhance membrane expression (Canti et al., 2005; Hoppa et al., 2012). Mean current density of channels co-expressed with p.R596P was

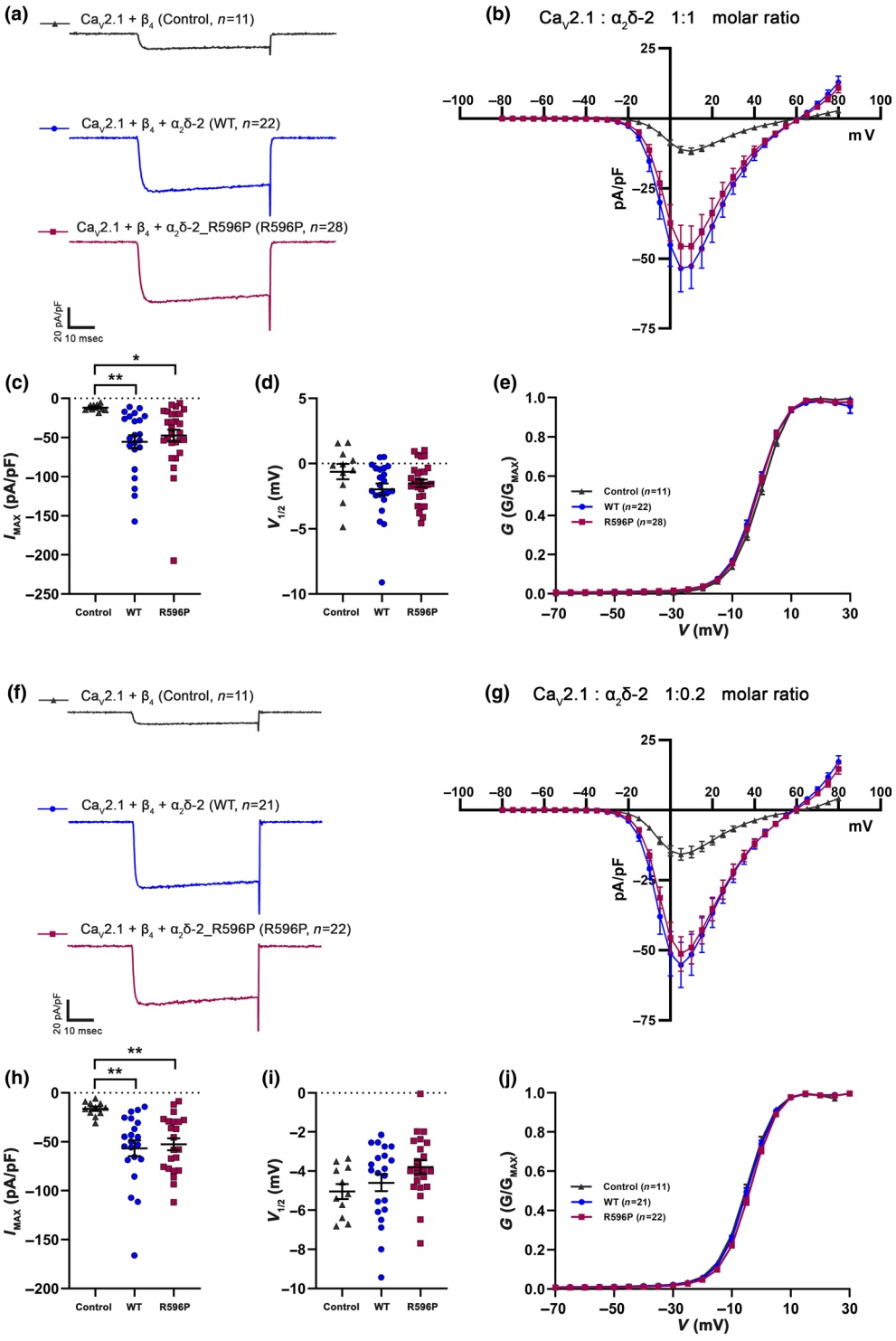

not significantly different from that of channels co-expressed with $\alpha_2\delta$-2_ΔMIDAS (Figure 3h; Table 3). However, there was a statistically significant difference in the half-maximal activation potential (Figure 3i; Table 3). Moreover, in 62% of cells co-transfected with $\alpha_2\delta$-2_ΔMIDAS, no current could be detected. In contrast, only 35% and 13% of cells co-transfected with p.R596P and WT $\alpha_2\delta$-2, respectively, showed no current [n numbers: $\alpha_2\delta$-2_ΔMIDAS (45), $\alpha_2\delta$-2_ R596P (40), and WT (53)]. Together, these data suggest that in contrast to $\alpha_2\delta$-2_ΔMIDAS, $\alpha_2\delta$-2_R596P proteins, despite showing a strongly reduced membrane expression, can still interact and modulate $Ca_V1.3$ channels at a very basic level.

3.4 | The p.R596P mutation does not compromise current properties of the P/Q-type channel $Ca_V2.1$

We next tested the consequences of the p.R596P mutation on the biophysical properties of Ca^{2+} currents mediated by the P/Q-type

FIGURE 4 The p.R596P mutation does not compromise the current properties of the P/Q-type channel $Ca_V2.1$. (a–j) Current properties of $Ca_V2.1$ recorded from tsA201 cells transfected with $Ca_V2.1$ and β_4 alone as a control (control, gray triangles), together with WT (WT, blue circles), or mutated $\alpha_2\delta$-2 (R596P, pink rectangles). (a–e) Recordings obtained from tsA201 cells transfected with the three subunits $Ca_V2.1/\beta_4/\alpha_2\delta$-2 in a molar ratio of 1:1:1, while (f–j) are recordings obtained from tsA201 cells transfected with the three subunits in a molar ratio of 1:1:0.2. Fifty msec test pulses from a holding potential of −80 mV to +80 mV were applied in 5 mV increments. (a, f) Representative whole-cell Ca^{2+} current traces at V_{MAX}. Current–voltage relationships (b, g), mean peak current densities (c, h), and mean half-maximal activation potentials (d, i). **Statistics**: (c, d) One-way ANOVA with Tukey's multiple-comparison test was performed on 11–28 recordings per condition obtained from three independent experiments. (c) Maximal current density, $F_{(2,58)}=5.5$; $p=0.0067$. *P*-values of the post hoc test for the respective comparisons: $P=0.01$ for control versus WT, $p=0.02$ for control versus R596P, and $p=0.72$ for WT versus R596P. (d) Half-maximal activation potential, $F_{(2,58)}=2.0$; $p=0.15$. *P*-values of the post hoc test for the respective comparisons: $P=0.12$ for control versus WT, $p=0.37$ for control versus R596P, and $p=0.65$ for WT versus R596P. (h, i) One-way ANOVA with Tukey's multiple-comparison test was performed on 11–22 recordings per condition obtained from three independent experiments. (h) Maximal current density, $F_{(2,51)}=7.4$; $p=0.0016$. *P*-values of the post hoc test for the respective comparisons: $P=0.002$ for control versus WT, $p=0.005$ for control versus R596P, and $p=0.89$ for WT versus R596P. (i) Half-maximal activation potential, $F_{(2,51)}=2.2$; $p=0.117$. P-values of the post hoc test for the respective comparisons: $P=0.76$ for control versus WT, $p=0.13$ for control versus R596P, and $p=0.29$ for WT versus R596P. Significances of post hoc tests between conditions are indicated in the graphs by asterisks (**$p<0.01$, *$p=0.02$).

TABLE 4 Current properties of $Ca_V2.1$ in tsA201 cells.

	$Ca_V2.1/\beta_4/\alpha_2\delta$-2 (1:1:1 molar ratio)			$Ca_V2.1/\beta_4/\alpha_2\delta$-2 (1:1:0.2 molar ratio)		
	Control	WT	R596P	Control	WT	R596P
Current density (pA/pF)	−11.9 ± 1.1	−55.5 ± 8.5	−47.4 ± 7.6	−16.3 ± 2.2	−56.6 ± 8.0	−52.5 ± 6.1
$V_{1/2}$ (mV)	−0.6 ± 0.5	−1.9 ± 0.4	−1.5 ± 0.2	−5.0 ± 0.3	−4.5 ± 0.4	−3.8 ± 0.3
V_{rev} (mV)	47.0 ± 0.5	44.7 ± 0.3	46.0 ± 0.3	44.4 ± 1.0	44.8 ± 0.4	45.7 ± 0.4
n	11	22	28	11	21	22

Note: All values are presented as mean ± SEM and were obtained from three independent experiments. $V_{1/2}$ and V_{rev} parameters were obtained from fitting the *I–V* curves to a Boltzmann function. $V_{1/2}$, half maximal activation potential; V_{rev}, extrapolated reversal potential; *n*, number of recordings. For statistics see Figure 4.

channel $Ca_V2.1$. Compared to the control condition without $\alpha_2\delta$-2, co-expression of $Ca_V2.1$ and β_4 together with the p.R596P mutant resulted in a fivefold increased current density. This increase was basically indistinguishable from the positive control group (co-expression of WT $\alpha_2\delta$-2, Figure 4a–e; Table 4), suggesting that $Ca_V2.1$ function is not compromised by the mutation. However, because $Ca_V2.1$ channels showed an upper limit of membrane expression in superior cervical ganglion neurons (Scott & Kammermeier, 2017), small changes in current densities may be masked. This prompted us to repeat the analysis of P/Q-type currents in tsA201 cells transfected with a molar ratio of 1:0.2 (α_1:$\alpha_2\delta$-2) instead of 1:1. However, also the low amount of $\alpha_2\delta$-2 cDNA used in these transfections neither resulted in a reduced $Ca_V2.1$ current density upon co-expression of WT $\alpha_2\delta$-2, or upon co-expression of mutated $\alpha_2\delta$-2 (Figure 4f–j; Table 4). Together this shows that $\alpha_2\delta$-2_R596P, despite showing an extremely low membrane expression, is still able to increase the functional membrane expression of $Ca_V2.1$ channels.

3.5 | Strongly reduced neuronal surface expression and presynaptic targeting of epitope-tagged $\alpha_2\delta$-2_R596P

So far, we studied the functional consequences of the p.R596P mutation in $\alpha_2\delta$-2 on the membrane expression and Ca^{2+}-channel properties upon heterologous expression in tsA201 cells. While this expression system is ideally suited to study the consequences of the mutated $\alpha_2\delta$-2 protein on distinct α_1 subunits and in the absence of endogenously expressed auxiliary subunits, it is essential to investigate the behavior and the consequences of the mutated protein in its native environment, namely neurons of the CNS. Therefore, we homologously expressed HA epitope-tagged WT or mutated $\alpha_2\delta$-2 together with soluble eGFP in mouse cultured hippocampal neurons. Live-cell immunostaining revealed that, similar to heterologous expression, $\alpha_2\delta$-2_R596P showed a strongly reduced surface expression compared to WT $\alpha_2\delta$-2, in all three main neuronal compartments, the soma, dendrites, and axons (Figure 5a).

As $\alpha_2\delta$-2 is particularly expressed in presynaptic terminals (Geisler et al., 2019), we next analyzed the presynaptic localization of $\alpha_2\delta$-2_R596P. To this end, presynaptic boutons were identified by the clustering of synapsin protein within axonal varicosities as visualized by the eGFP fluorescence. Analysis of presynaptic boutons expressing HA-tagged $\alpha_2\delta$-2 proteins revealed a presynaptic localization of $\alpha_2\delta$-2_R596P, similar to WT $\alpha_2\delta$-2 (Figure 6a), as indicated by the colocalization and the line scan analysis of the 2HA-$\alpha_2\delta$-2 (red), synapsin (blue), and eGFP (green) staining pattern of representative images (Figure 6b). However, quantitative analysis revealed that, compared to WT $\alpha_2\delta$-2, overall presynaptic targeting of $\alpha_2\delta$-2_R596P was strongly reduced (Figure 6d).

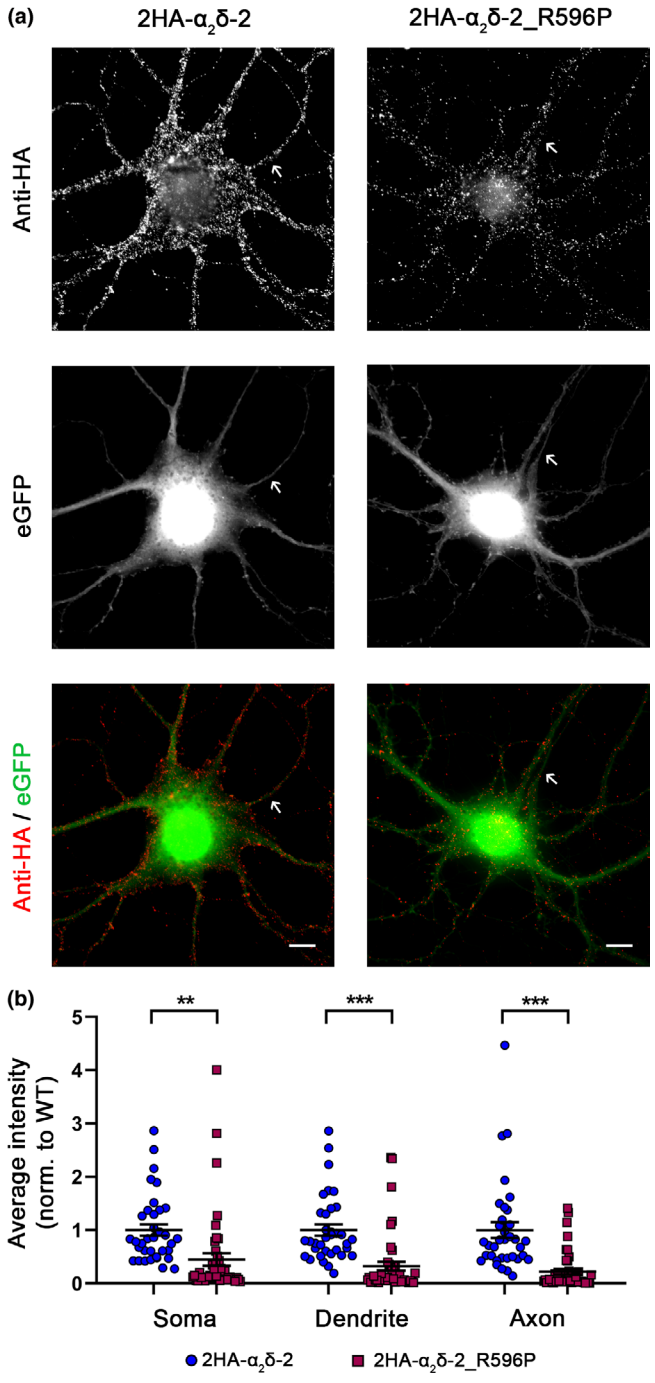

FIGURE 5 Strongly reduced membrane expression of $\alpha_2\delta$-2_R596P in differentiated cultured hippocampal neurons. (a) Representative examples of primary cultured hippocampal neurons transfected with soluble eGFP together with either HA-tagged WT (2HA-$\alpha_2\delta$-2) or mutated (2HA-$\alpha_2\delta$-2_R596P) $\alpha_2\delta$-2. Anti-HA live-cell labeling demonstrates a reduced staining intensity of $\alpha_2\delta$-2_R596P in the soma, dendrites, and the axon (indicated by an arrow) compared to WT $\alpha_2\delta$-2. (b) Quantification of the average HA fluorescent intensities in the three compartments shows that the surface expression of mutated $\alpha_2\delta$-2 is strongly reduced compared to WT $\alpha_2\delta$-2. Graphs show values for individual cells (dots) and mean ± SEM (lines). All values were normalized to the mean of the WT 2HA-$\alpha_2\delta$-2 fluorescence intensity within each culture preparation. Data were obtained from three independent culture preparations; 35 and 45 cells expressing WT or mutated HA-tagged $\alpha_2\delta$-2 were analyzed, respectively. **Statistics**: Unpaired *t*-test, soma: $T_{(78)} = 3.4$; $^{**}p = 0.0011$, dendrite: $T_{(78)} = 5.1$; $^{***}p < 0.0001$, axon: $T_{(78)} = 5.5$; $^{***}p < 0.0001$. Scale bars, 10 µm.

3.6 | Homologous expression of WT or R596P-mutated $\alpha_2\delta$-2 differentially affects presynaptic differentiation

The unaltered $Ca_V2.1$ current observed when p.R596P was co-expressed with the channel in tsA201 cells (Figure 4) suggests that despite the strong reduction in membrane expression, the p.R596P mutant was still able to traffic $Ca_V2.1$ channels to the plasma membrane. However, and as discussed above, $Ca_V2.1$ channel membrane expression ceiling may obscure small differences in channel modulation. It has previously been shown that homologous expression of $\alpha_2\delta$-1 in cultured neurons increases synaptic $Ca_V2.1$ channel clustering (Ablinger et al., 2022; Hoppa et al., 2012). Here, we show that WT $\alpha_2\delta$-2 similarly induces an increase in endogenous $Ca_V2.1$ clustering at presynaptic terminals compared to control neurons expressing eGFP alone (Figure 7a,c). This observation allowed us to test, whether this property of $\alpha_2\delta$-2 is compromised by the mutation. In contrast to WT $\alpha_2\delta$-2, $\alpha_2\delta$-2_R596P expression resulted only in a slight but not significant increase in presynaptic $Ca_V2.1$ expression (Figure 7c), which is neither different from control (eGFP alone) nor from WT $\alpha_2\delta$-2 (WT). Surprisingly, however, homologous expression of $\alpha_2\delta$-2_R596P significantly reduced presynaptic synapsin clustering, which was not observed in the control groups (eGFP or WT $\alpha_2\delta$-2; Figure 7d). The reduction in synapsin expression was not the consequence of an altered bouton size, as evidenced by quantitative analysis of the size of eGFP-positive varicosities (Figure 7e). Moreover, the decrease in presynaptic synapsin clustering suggests that the p.R596P mutant, despite its low membrane expression, competes with endogenously expressed $\alpha_2\delta$ proteins ($\alpha_2\delta$-1 to -3), thereby mediating a dominant-negative effect resulting in defective presynaptic differentiation.

3.7 | The p.R596P mutation affects the ability of $\alpha_2\delta$-2 to increase presynaptic calcium transients

Homologous expression of $\alpha_2\delta$-2_R596P fails to induce a significant increase in presynaptic $Ca_V2.1$ channel abundance. This is in contrast to the unaltered biophysical current properties (confer Figure 4) and hence suggests a mild disruption in the interaction of $\alpha_2\delta$-2 with $Ca_V2.1$. Moreover, the decrease in presynaptic synapsin clustering is a sign of defective presynaptic differentiation, which, in theory, can also affect the expression of other presynaptic Ca_V channel isoforms. Therefore, we next tested whether and to what extent presynaptic Ca^{2+} transients were affected by WT or R596P $\alpha_2\delta$-2. To this end, cultured hippocampal neurons were transfected with the genetically encoded GCaMP6f Ca^{2+} indicator coupled to synaptophysin [SynGCaMPF6f; Brockhaus et al., 2019)], together with soluble

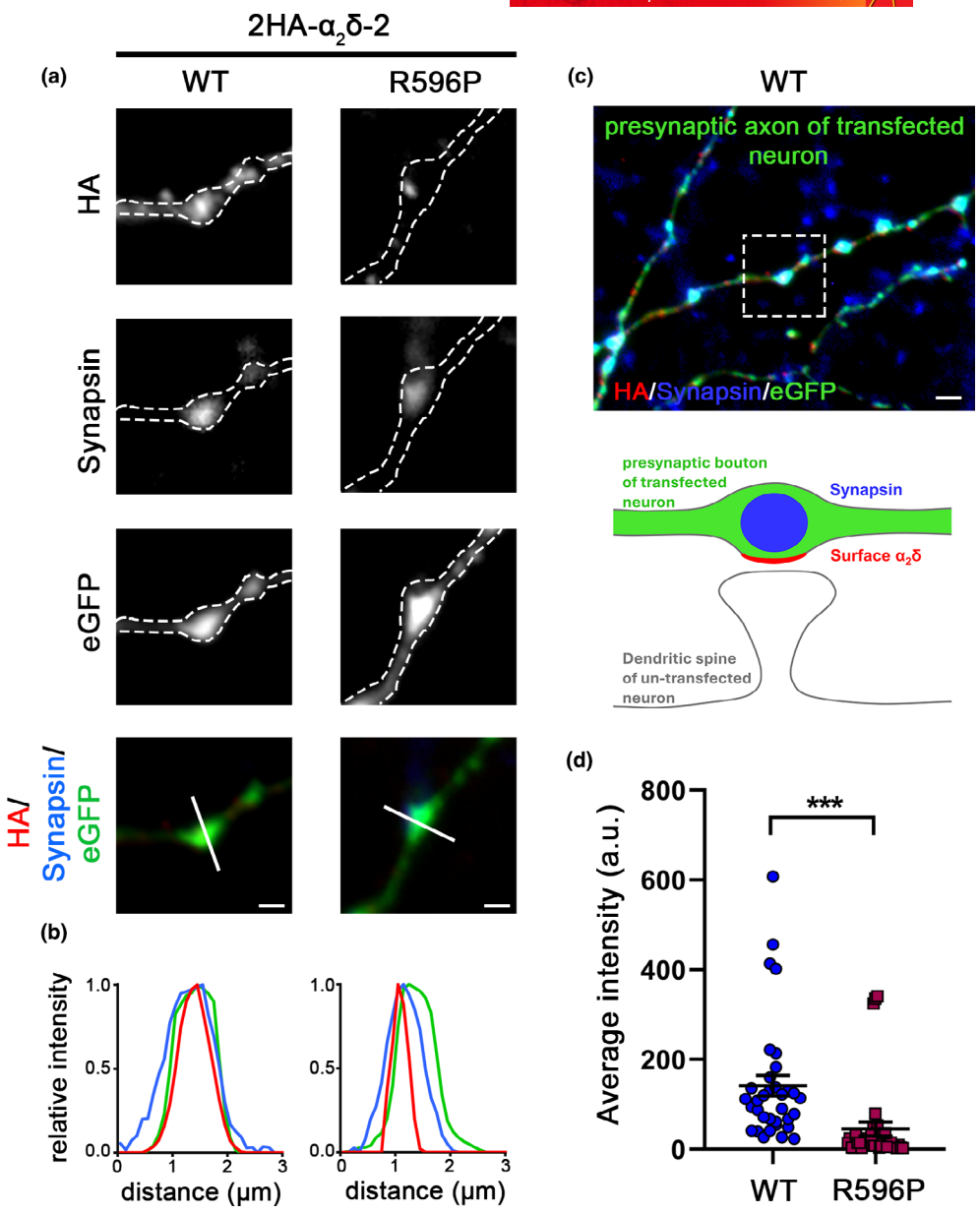

FIGURE 6 Reduced presynaptic targeting of $\alpha_2\delta$-2_R596P. (a) Representative presynaptic boutons of transfected cultured hippocampal neurons, identified by the eGFP expression and synapsin clustering, are outlined by a dashed line. Live-cell staining shows that $\alpha_2\delta$-2_R596P is expressed at the surface of presynaptic boutons. Scale bars, 1 μm. (b) Line scan analysis of 2HA-$\alpha_2\delta$-2 (red), synapsin (blue), and eGFP (green) staining pattern of representative images supports a presynaptic localization by the overlapping peaks of HA-label (red) in relation to synapsin (blue) and eGFP (green). (c) The surrounding region of the selected WT synapse in (a) and a sketch summarizing the observed labeling pattern. Scale bar, 2 μm. (d) Average fluorescence intensity measurements of the HA signal in positively transfected boutons revealed a strong reduction in presynaptic localization of $\alpha_2\delta$-2_R596P compared to WT $\alpha_2\delta$-2. **Statistics**: Graph shows mean values of minimally five synapses for individual cells (dots) and means ± SEM (lines). Data were obtained from three independent culture preparations and 34 and 35 cells expressing WT or mutated HA-tagged $\alpha_2\delta$-2 were analyzed, respectively. Statistics: unpaired two-tailed *t*-test, $t_{(67)} = 3.0$; $^{***}p = 0.0037$.

mCherry (Figure 8a). Comparable synaptic expression of GCaMP6f across conditions was confirmed by analyzing the fluorescent signal intensity in synaptic boutons at baseline (control: 40.37 ± 2.59, WT: 35.31 ± 0.86, R596P: 38.35 ± 1.54; one-way ANOVA with Tukey's multiple-comparison test: $F_{(2,65)} = 2.14$, $p = 0.13$). Consistent with previous findings, WT $\alpha_2\delta$-2 increased presynaptic peak Ca^{2+} amplitudes in response to 1 and 10 action potentials (AP) triggered by field stimulation at a frequency of 50 Hz (Figure 8b–e). This was evident when plotting the mean traces (Figure 8b,d) and by analyzing the peak Ca^{2+} signals of all individual cells (Figure 8c,e). Surprisingly, the p.R596P mutant also increased presynaptic peak Ca^{2+} amplitudes similar to WT $\alpha_2\delta$-2 in response to 1 AP (Figure 8b,c). However, in response to 10 Aps, the mean peak Ca^{2+} amplitude of the p.R596P condition is lower, albeit not significantly different, compared to the

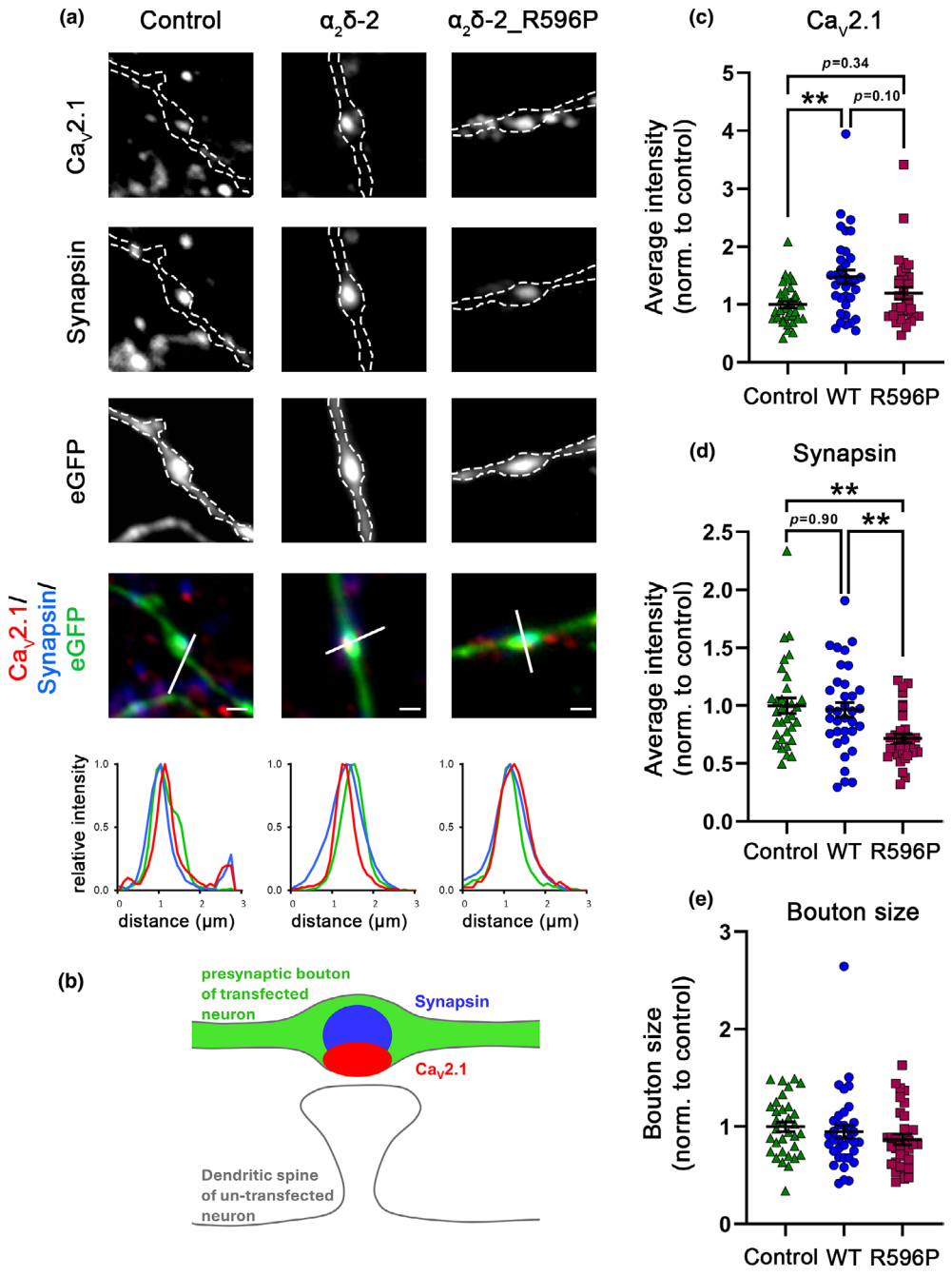

FIGURE 7 Homologous expression of $\alpha_2\delta$-2_R596P in hippocampal neurons fails to induce a statistically significant increase in presynaptic $Ca_V2.1$ clustering and decreases presynaptic synapsin abundance. (a) Representative micrographs of presynaptic boutons of cultured hippocampal neurons transfected with eGFP alone (control) or co-transfected together with either WT ($\alpha_2\delta$-2) or mutated ($\alpha_2\delta$-2_R596P) $\alpha_2\delta$-2. Immunofluorescent signals of $Ca_V2.1$ channels colocalize with presynaptic synapsin clusters (see also co-localizing peaks of fluorescence signals in line scan analysis). (b) Sketch depicting the expected staining pattern in (a). (c) Quantification of presynaptic $Ca_V2.1$ cluster intensity shows that contrary to WT, presynaptic expression of the p.R596P mutant fails to induce a significant increase in presynaptic $Ca_V2.1$ clustering. (d) Quantification of presynaptic synapsin abundance shows a strong reduction in synaptic synapsin intensity upon expression of the p.R596P mutant. (e) Quantification of boutons size, as identified by the eGFP fluorescence area, shows no difference between the different experimental conditions. **Statistics**: Graphs of $Ca_V2.1$ and synapsin average intensities and bouton size show values for individual cells (dots) and means ± SEM (lines). Cells were obtained from three independent culture preparations. One-way ANOVA with Tukey's multiple-comparison test. A total of 33–35 cells per condition, (c) $F_{(2,98)} = 6.1$, $^{**}p = 0.0031$. *P*-values of the post hoc test for the respective pairwise comparisons: $P = 0.002$ for control versus WT, $p = 0.34$ for control versus R596P, and $p = 0.12$ for WT versus R596P. (d) $F_{(2,98)} = 7.0$, $^{**}p = 0.0013$. *P*-values of the post hoc test for the respective pairwise comparisons: $P = 0.89$ for control versus WT, $p = 0.002$ for control versus R596P, and $p = 0.01$ for WT versus R596P. (e) $F_{(2,98)} = 1.2$, $p = 0.29$. *P*-values of the post hoc test for the respective pairwise comparisons: $P = 0.81$ for control versus WT, $p = 0.27$ for control versus R596P, and $p = 0.61$ for WT versus R596P. Significances of post hoc tests between conditions are indicated in the graphs by asterisks ($^{**}p < 0.01$). Scale bar, 1 µm.

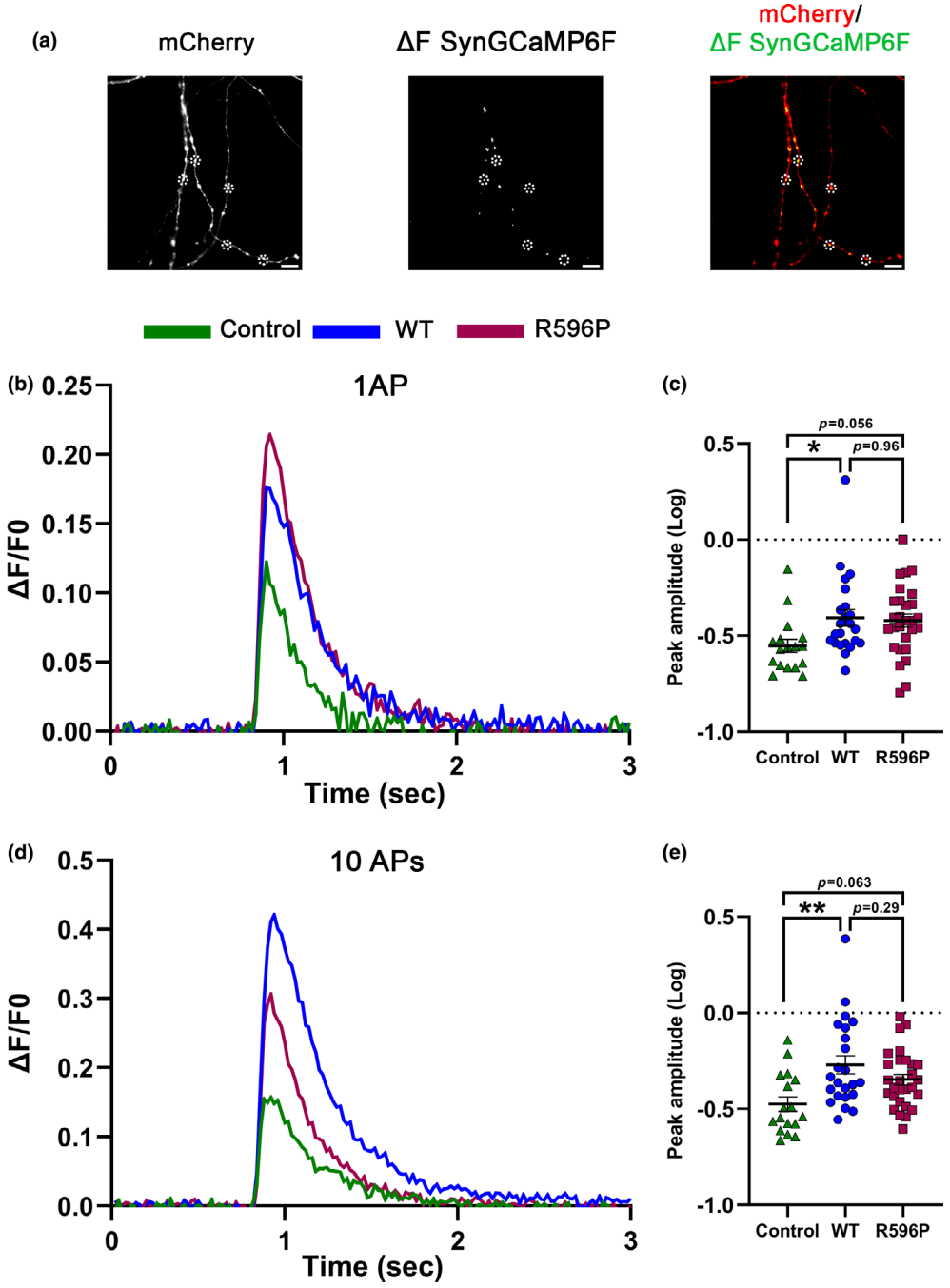

FIGURE 8 Presynaptic Ca^{2+} transients of neurons expressing WT $\alpha_2\delta$-2 and $\alpha_2\delta$-2_R596P in comparison with control neurons. (a) Fluorescent micrographs of representative presynaptic varicosities identified by the mCherry fluorescence. The presynaptic Ca^{2+} signal (ΔSynGCaMP6f) was calculated by subtracting the control SynGCaMP6f fluorescence at baseline from the SynGCaMP6f fluorescence at the maximal response. Scale bar 5 μm. Mean fluorescence traces (b, d), and quantification of the peak fluorescence (c, e) of presynaptic Ca^{2+} signals (ΔF/F of SynGCaMP6f) elicited by 1 action potential (AP), or 10 APs at 50 Hz stimulations, in cultured hippocampal neurons co-transfected with SynGCaMP6f and mCherry alone (control, green, triangles) or together with either WT (WT, blue, circles) or mutated $\alpha_2\delta$-2 (R596P, pink, rectangles). (b, d) Lines show the mean fluorescence traces from 17 to 28 cells per condition from four independent culture preparations. Quantification of peak fluorescent amplitudes (log) in response to stimulations with 1 (c) or 10 APs (e) shows values for individual cells (symbols) and means ± SEM (lines). Each symbol represents the mean peak fluorescence signal of 20 synapses measured from one neuron. **Statistics**: One-way ANOVA with Tukey's multiple-comparison test: 1 AP: $F_{(2,65)}=3.6$, $p=0.038$. *P*-values of the post hoc test for the respective pairwise comparisons: $P=0.03$ for control versus WT, $p=0.06$ for control versus R596P, and $p=0.96$ for WT versus R596P. 10 AP: $F_{(2,65)}=6.2$, $p=0.003$. *P*-values of the post hoc test for the respective pairwise comparisons: $P=0.002$ for control versus WT, $p=0.06$ for control versus R596P, and $p=0.28$ for WT versus R596P. Significances of post hoc tests between conditions are indicated in the graphs by asterisks ($^{**}p<0.01$, $^{*}p=0.038$).

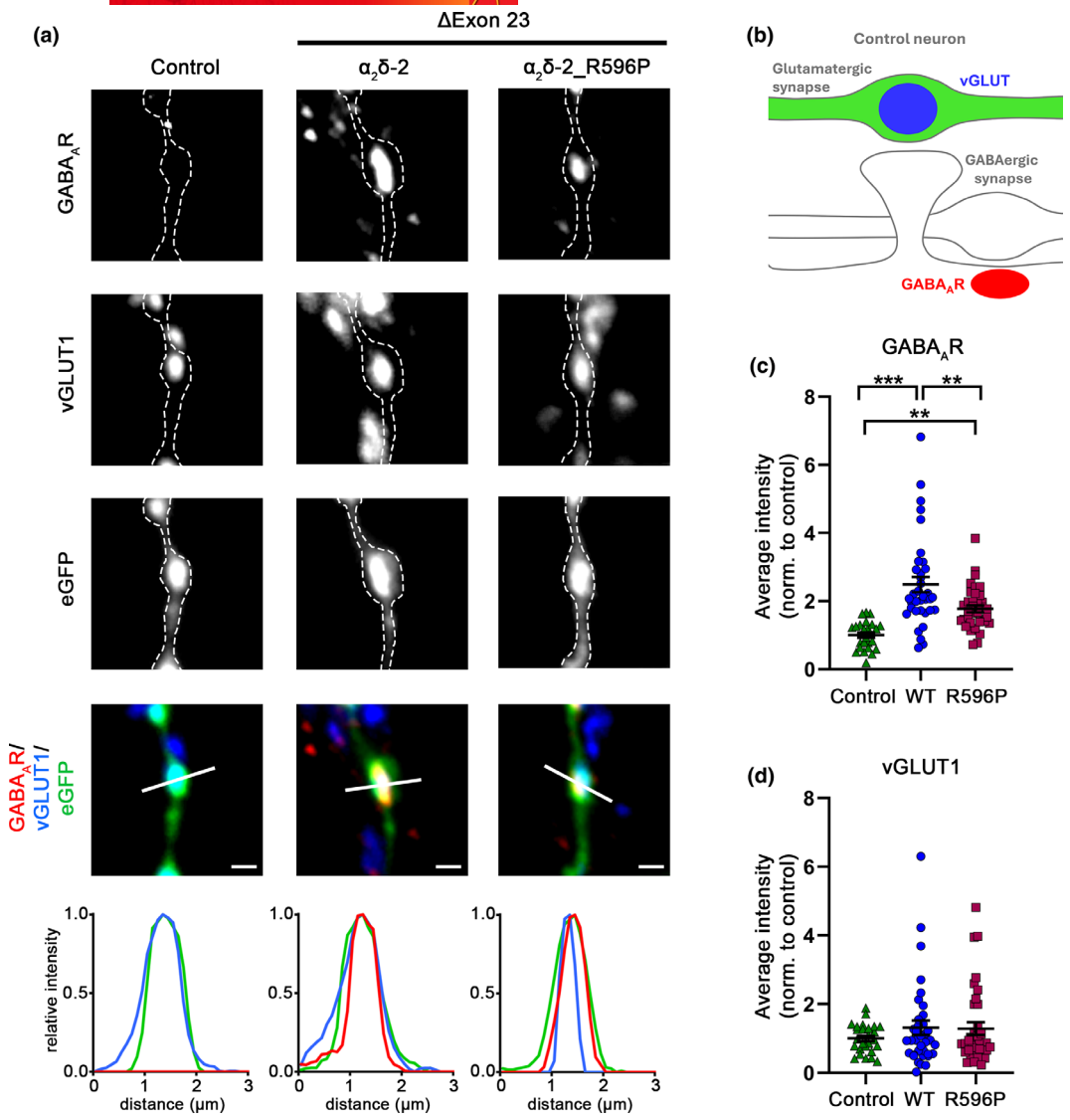

FIGURE 9 Reduced trans-synaptic coupling to postsynaptic $GABA_AR$ of the $\alpha_2\delta$-2_R596P mutant. immunofluorescent labeling of presynaptic vGLUT1 and postsynaptic $GABA_AR$ was used to identify the formation of mismatched synapses in hippocampal neurons transfected with soluble eGFP as control or together with either WT or mutated $\alpha_2\delta$-2_ΔE23. (a) Both, homologous over-expression of WT and mutated $\alpha_2\delta$-2 lead to the formation of mismatched synapses. However, compared to WT $\alpha_2\delta$-2, neurons transfected with $\alpha_2\delta$-2_R596P mutant showed a reduced postsynaptic $GABA_AR$s recruitment, as detected by postsynaptic $GABA_AR$ clusters opposite vGLUT1-positive glutamatergic terminals (a, $\alpha_2\delta$-2, $\alpha_2\delta$-2_R596P). Colocalization of the fluorescence signals of representative images was analyzed using line scans. (b) Sketch summarizing the observed labeling pattern of a control bouton expressing eGFP alone. In control boutons, potential glutamatergic synapses are positive for presynaptic vGLUT1 (blue) but negative for postsynaptic $GABA_AR$s (red); in contrast to glutamatergic synapses, GABAergic synapses are typically located along the dendritic shaft. Quantifications of immunofluorescence intensities of $GABA_AR$ (c) and vGLUT1 (d) labeling show values for individual cells (dots) and means ± SEM (lines). Values were normalized to the fluorescent intensities of the control condition within each culture preparation. Cells were obtained from three independent culture preparations. **Statistics**: ANOVA with Tukey's multiple-comparison test was performed on 26–37 cells per condition. $GABA_AR$: $F_{(2,96)}=20.06$; $p<0.0001$. *P*-values of the post hoc test for the respective pairwise comparisons: $P<0.0001$ for control versus WT, $p=0.003$ for control versus R596P, and $p=0.003$ for WT versus R596P. vGLUT1: $F_{(2,96)}=0.81$; $p=0.45$. *P*-values of the post hoc test for the respective pairwise comparisons: $P=0.47$ for control versus WT, $p=0.53$ for control versus R596P, and $p=0.99$ for WT versus R596P. Significances of post hoc tests between conditions are indicated in the graphs by asterisks (***$p<0.001$, **$p<0.01$). Scale bars, 1 μm.

WT $\alpha_2\delta$-2 condition. Moreover, and in contrast to WT $\alpha_2\delta$-2, the mean peak amplitude was only approaching statistically significant difference from control neurons (Figure 8b–e). This suggests that homologous expression of $\alpha_2\delta$-2_R596P less efficiently enhances presynaptic Ca^{2+} transients than expression of WT $\alpha_2\delta$-2.

3.8 | Trans-synaptic signaling of $\alpha_2\delta$-2_R596P

Presynaptic over-expression of a splice variant of $\alpha_2\delta$-2 lacking exon 23 (E23) in hippocampal neurons has previously been shown to induce aberrant axonal wiring resulting in a mismatched

localization of postsynaptic $GABA_A$ receptors ($GABA_AR$) opposite glutamatergic nerve terminals (Geisler et al., 2019). E23 is located downstream of R596 and codes for eight amino acids following residue 664. Structural homology modeling suggested that exclusion of this exon leads to the formation of an α-helix (Geisler et al., 2019). To test whether introduction of the p.R596P mutation alters the trans-synaptic function of $\alpha_2\delta$-2, we quantified the expression levels of postsynaptic $GABA_AR$ opposite mismatched vGLUT1-containing presynaptic boutons upon homologous overexpression of WT or mutated $\alpha_2\delta$-2_ΔE23 compared to neurons expressing eGFP alone as control. As shown previously (Ablinger et al., 2022; Geisler et al., 2019), WT $\alpha_2\delta$-2_ΔE23 induces clustering of postsynaptic $GABA_AR$ opposite vGLUT1-positive terminals (Figure 9a,c, $\alpha_2\delta$-2 and WT, respectively). Neurons transfected with $\alpha_2\delta$-2_ΔE23_R596P were able to recruit $GABA_ARs$ opposite glutamatergic nerve terminals (Figure 9a,c), however, $GABA_ARs$ clustering was significantly reduced compared to WT $\alpha_2\delta$-2. This was particularly evident when quantifying the immunofluorescent signal of average fluorescence intensity of postsynaptic $GABA_ARs$. Because of the strong reduction in presynaptic expression of the R596P mutant (see above), a reduced trans-synaptic action was to be expected. However, it is important to note that presynaptic expression is strongly reduced to 31% (confer Figure 6), while the trans-synaptic recruitment of postsynaptic $GABA_ARs$ is reduced to only 73% (confer Figure 9). Together this suggests that even small amounts and/or less stably expressed $\alpha_2\delta$-2 proteins can mediate a trans-synaptic function.

The aberrant wiring and postsynaptic $GABA_AR$ recruitment by presynaptic $\alpha_2\delta$-2_ΔE23 was associated with reduced glutamatergic synaptic transmission (Geisler et al., 2019). Hence, to further assess the trans-synaptic consequences of $\alpha_2\delta$-2_R596P compared to WT $\alpha_2\delta$-2, we recorded and analyzed spontaneous miniature excitatory postsynaptic currents (mEPSCs). To ensure a uniform expression of the transfected $\alpha_2\delta$-2_ΔE23 cDNAs in all neurons (Figure 10a), we here used lentivirus-mediated transfection. This is in contrast to the above-mentioned experiments, in which liposomal-mediated transfection was employed to obtain a low transfection efficiency of isolated presynaptic neurons. As expected for aberrantly wired synapses, both WT and mutated $\alpha_2\delta$-2 decreased the frequency of mEPSCs compared to neurons infected with eGFP-expressing lentiviral particles only (control) (Figure 10b,d). However, consistent with the observed differences in postsynaptic $GABA_AR$ recruitment (confer Figure 9c), WT $\alpha_2\delta$-2 resulted in a larger decrease in mEPSCs frequency (on average reduction by ~50%; mean ± SEM: 0.51 ± 0.05) compared to the mutated $\alpha_2\delta$-2 (on average reduction by ~30%; mean ± SEM: 0.73 ± 0.08). An efficient and synchronized synaptic transmission requires precisely matched and aligned pre- and postsynaptic proteins. Hence, our data suggest that the strong reduction in mEPSC frequency is the result of a reduced number of functional synapses caused by the aberrant wiring of glutamatergic boutons with GABAergic postsynaptic sites. Interestingly, however, we also observed differences between the experimental conditions in the amplitude of the mEPSC, which is an indirect measure of postsynaptic AMPA receptor expression. The mean amplitude of mEPSCs recorded in neurons expressing mutated $\alpha_2\delta$-2 was significantly reduced by ~24%. In contrast, we did not observe a reduction in mEPSC amplitudes in neurons infected with WT $\alpha_2\delta$-2. Cumulative frequency distribution of mEPSC amplitudes (Figure 10e) and analysis of all individual mEPSC events (Figure 10f) show an even more prominent reduction of the mEPSC amplitude of neurons with R596P in comparison with control and WT $\alpha_2\delta$-2. Together, this shows that the decrease in mEPSC amplitude was not solely caused by altered wiring, but in the case of the mutated $\alpha_2\delta$-2 protein, it rather reflects an independent underlying mechanism.

4 | DISCUSSION

Here, we provide a functional characterization of a potential disease-causing CACNA2D2 mutation, which focuses not only on the Ca^{2+} channel-dependent functions of $\alpha_2\delta$-2 but also on synaptic and trans-synaptic functions of $\alpha_2\delta$ proteins. The p.R596P mutation decreases membrane expression and synaptic targeting of $\alpha_2\delta$-2. This defect in membrane expression differentially affects L-type and non-L-type Ca^{2+} channels: while the p.R596P mutation alters current densities and voltage dependence of activation of the postsynaptic L-type channel $Ca_V1.3$ upon heterologous co-expression, it has no effect on current properties of the presynaptic P/Q-type channel $Ca_V2.1$. However, in comparison with WT $\alpha_2\delta$-2 expression, $\alpha_2\delta$-2_R596P in hippocampal neurons did not significantly increase the presynaptic abundance of endogenously expressed $Ca_V2.1$ channels and limited its capacity to increase presynaptic Ca^{2+} transients, even though there was no difference between the means of WT and R596P $\alpha_2\delta$-2. Despite the low membrane expression, $\alpha_2\delta$-2_R596P could still mediate trans-synaptic signaling to postsynaptic $GABA_ARs$. Finally, homologous expression of mutated $\alpha_2\delta$-2 results in a defective presynaptic differentiation indicated by decreased presynaptic synapsin clustering, and altered postsynaptic differentiation indicated by reduced mEPSCs amplitudes.

4.1 | R596 is critical for membrane expression of $\alpha_2\delta$-2

$\alpha_2\delta$ proteins, in their capacity as Ca^{2+} channel subunits, play an important role in membrane trafficking of the channel complex. However, $\alpha_2\delta$ proteins can also reach the cell surface independently of the VGCC complex (Canti et al., 2005; Cassidy et al., 2014; Schredelseker et al., 2005). Structural homology modeling of $\alpha_2\delta$-2 predicts one critical interaction of the highly conserved R596 with Y1094 within the δ peptide. Hence, R596 is predicted to maintain the interaction between α_2 and δ peptides and thereby stabilize the whole structure of $\alpha_2\delta$-2. Indeed, $\alpha_2\delta$-2_R596P shows a reduced

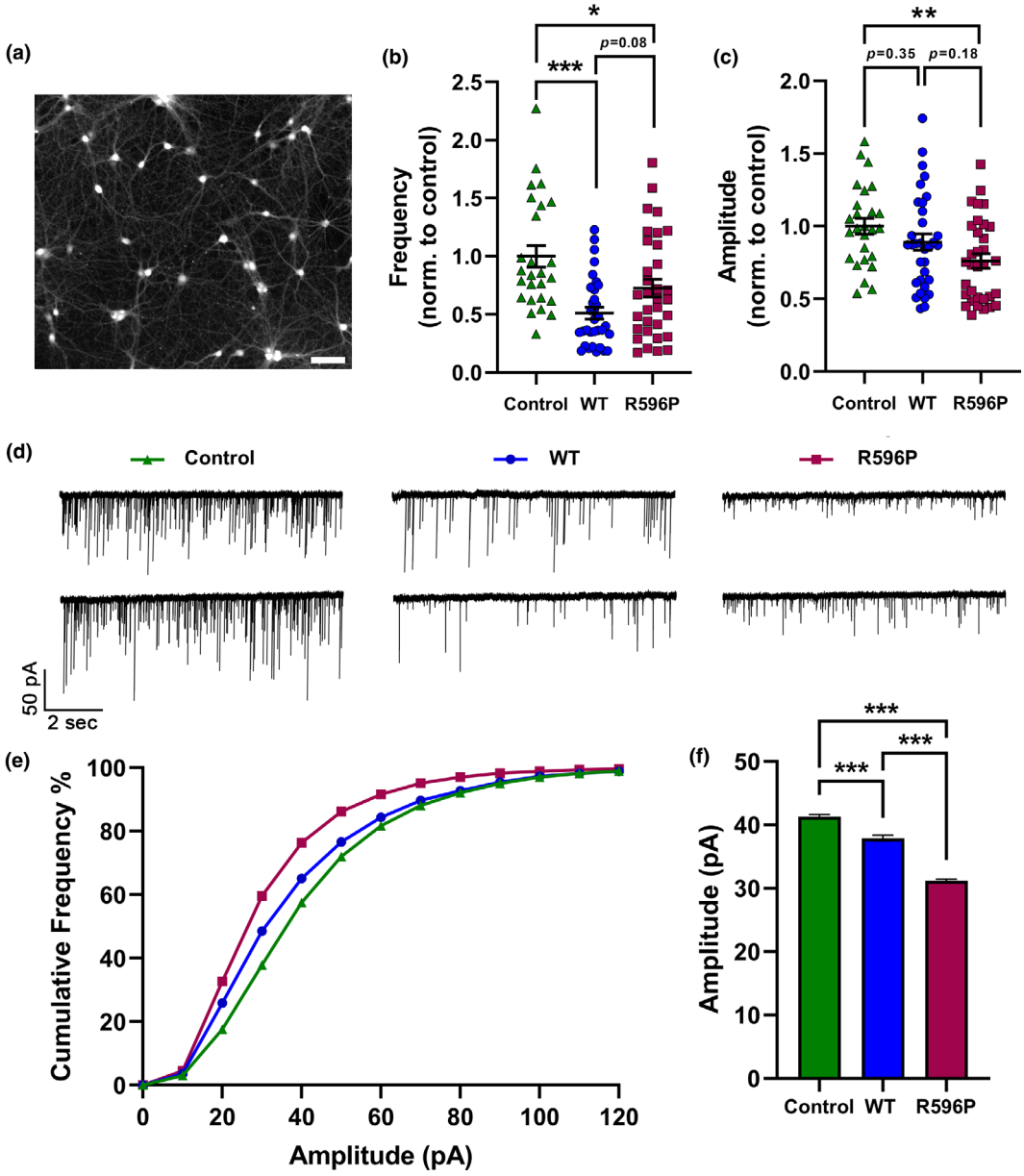

FIGURE 10 Homologous expression of $\alpha_2\delta$-2_R596P resulted in a greater reduction in spontaneous glutamate-mediated synaptic transmission. Recordings of mEPSCs in 14–15 DIV cultured hippocampal neurons expressing soluble eGFP alone (control, green triangles), and either WT (WT, blue circles) or mutated (R596P, pink rectangles) $\alpha_2\delta$-2_ΔE23. (a) Representative image of hippocampal neurons at DIV 15 infected with $\alpha_2\delta$-2_R596P showing a ~100% infection efficiency. Scale bar, 200 µm. Quantification of mEPSC frequencies (b) and average amplitudes (c). Amplitudes and frequencies of mEPSCs were normalized to the mean value of control condition for each individual experiment. (d) Two representative traces of mEPSCs from independent recordings for all three conditions. (e) Cumulative frequency distribution histograms of all mEPSC amplitudes recorded from neurons shown in the previous panels. Number of analyzed events per condition: Control, $n = 6012$; WT, $n = 3374$; R596P, $n = 5384$. (f) Comparison of mean mEPSC amplitudes of all recorded events. Expression of the R596P mutant was associated with larger reduction in mEPSC amplitude compared to WT $\alpha_2\delta$-2. Statistics: (b, c) One-way ANOVA with Tukey's multiple-comparison test was performed on 26–33 recordings per condition from three independent culture preparations. (b) Frequency: $F_{(2,89)} = 10.5$; $p < 0.0001$. *P*-values of the post hoc test for the respective pairwise comparisons: $P < 0.001$ for control versus WT, $p = 0.03$ for control versus R596P, and $p = 0.08$ for WT versus R596P. (c) Amplitude: $F_{(2,89)} = 4.7$; $p = 0.01$. P-values of the post hoc test for the respective pairwise comparisons: $P = 0.35$ for control versus WT, $p = 0.008$ for control versus R596P, and $p = 0.18$ for WT versus R596P (f) One-way ANOVA with Tukey's multiple-comparison test was performed on 3374–6012 mEPSC events, $F_{(2,14767)} = 273.6$, $p < 0.0001$. *P*-values of the post hoc test for the respective pairwise comparisons: $P < 0.0001$ for control versus WT, control versus R596P, and WT versus R596P. Significances of post hoc tests between conditions are indicated in the graphs by asterisks (***$p < 0.001$, **$p < 0.01$, *$p = 0.031$).

membrane expression both upon heterologous and homologous expression. Correct folding of membrane proteins in the endoplasmic reticulum (ER) following translation is crucial for the forward trafficking to the cell surface and aberrantly folded proteins are retained in the ER and may be subject to degradation (Vembar & Brodsky, 2008). However, this seems not to be the case for

$\alpha_2\delta$-2_R596P as total protein expression was not compromised by the mutation. Hence, the reduced membrane expression suggests that the p.R596P mutation either affects forward trafficking from the ER and/or increases the internalization rate caused by destabilization of the protein on the cell surface.

4.2 | The p.R596P mutation uncovers isoform- and cell-type-specific differences in $\alpha_2\delta$-2-mediated functions

All $\alpha_2\delta$ isoforms augment the Ca^{2+} currents of all Ca_V1 and Ca_V2 channels with little effect on the single-channel conductance (Barclay et al., 2001; Tuluc et al., 2007), implying that $\alpha_2\delta$ proteins mediate the current enhancement by mainly increasing the functional membrane expression of the channel complexes. While the exact underlying mechanisms remain elusive, a crucial role of the MIDAS motif within the VWA domain in membrane trafficking of the α_1 subunit seems likely (Canti et al., 2005). Our present data show that p.R596P differently affects the ability of $\alpha_2\delta$-2 to enhance Ca^{2+} currents of L-type (Ca_V1) and non-L-type (Ca_V2) channels upon heterologous co-expression. While the p.R596P mutation significantly reduced the current density and shifted the voltage dependence of activation to more depolarized potentials of $Ca_V1.3$ channels, it did not affect the biophysical properties of $Ca_V2.1$ channels. This differential effect could be attributed to two mechanisms: differences in the affinity between $\alpha_2\delta$-2 and α_1 isoforms (Voigt et al., 2016) or membrane expression ceiling effects of Ca_V2 channels (Scott & Kammermeier, 2017). The fact that $Ca_V2.1$ α_1, $\alpha_2\delta$-2, and β_4 are the dominating isoforms expressed in the cerebellum and that their expression levels co-increase during neuronal differentiation (Schlick et al., 2010) indicates endogenous complexing of these subunits. We can speculate that in contrast to $Ca_V1.3$, the affinity between $Ca_V2.1$ and $\alpha_2\delta$-2 could be strong enough to tolerate the p.R596P mutation as well as its reduced membrane expression. As Ca_V2 channels possess an upper limit of membrane expression (Cao et al., 2004; Scott & Kammermeier, 2017), it seems more likely that slight changes in current densities may be masked by this property. To test this, we reduced the amount of transfected $\alpha_2\delta$-2 WT and mutated cDNA by fivefold. However, also under this experimental paradigm, co-expression of $\alpha_2\delta$-2_R596P did not reduce the current density of $Ca_V2.1$ channels. This finding suggests that the mutation does not impede membrane trafficking of $Ca_V2.1$ channels in a heterologous expression system, and hence, it differentially affects L-type and non-L-type Ca^{2+} channels.

Because surface expression of $\alpha_2\delta$-2_R596P was also strongly reduced in hippocampal neurons, we next tested the consequence of the mutation on endogenous $Ca_V2.1$ channels in their native neuronal environment. An increase in presynaptic $Ca_V2.1$ clustering and presynaptic Ca^{2+} transients is a hallmark of homologous expression of $\alpha_2\delta$ isoforms in wild-type hippocampal neurons (Ablinger et al., 2022; Schopf et al., 2021). In contrast to heterologous co-expression, $\alpha_2\delta$-2_R596P did not increase presynaptic clustering of endogenous $Ca_V2.1$ channels and presynaptic Ca^{2+} transients to the same extent as WT $\alpha_2\delta$-2, whereby the means of WT and mutated $\alpha_2\delta$-2 were not significantly different. Altered modulation of endogenous $Ca_V2.1$ by mutated $\alpha_2\delta$-2 in synapses of differentiated hippocampal neurons uncovers cell-type-specific modulation by $\alpha_2\delta$ proteins which cannot be reconstituted in a heterologous expression system. Together, this suggests that modulation of Ca^{2+} channels by $\alpha_2\delta$-2 proteins is not limited to $\alpha_1/\alpha_2\delta$-2 protein–protein interactions but also involves the local macromolecular environment of a specialized cellular compartment such as the presynaptic terminal. Moreover, this finding highlights the importance of studying the mechanistic consequences of disease-associated mutations within their specific and native cellular environment.

4.3 | The p.R596P mutation affects pre- and postsynaptic differentiation by distinct mechanisms

$\alpha_2\delta$-2_R596P showed a reduced, albeit still functional, trans-synaptic recruitment of postsynaptic $GABA_AR$, a recently identified trans-synaptic function of $\alpha_2\delta$-1 and $\alpha_2\delta$-2 splice variants in both GABAergic and glutamatergic synapses (Ablinger et al., 2022; Geisler et al., 2019). It is still elusive whether this trans-synaptic function of $\alpha_2\delta$ is mediated by a direct trans-synaptic interaction or indirectly by the interaction with other synaptic organizers. On the one hand, the reduced trans-synaptic function of $\alpha_2\delta$-2_R596P together with its reduced surface expression point toward a direct trans-synaptic interaction. On the other hand, the fact that the effect on trans-synaptic $GABA_AR$ recruitment is much smaller than the reduction in presynaptic membrane expression of $\alpha_2\delta$-2_R596P indicates that even small amounts and/or less stably expressed $\alpha_2\delta$-2 proteins are sufficient for trans-synaptic signaling. Even though the trans-synaptic recruitment of $GABA_ARs$ and its consequence on synaptic transmission were observed in a non-physiologic experimental paradigm, namely the over-expression in glutamatergic neurons, it may provide important insights into potential physiological roles of $\alpha_2\delta$-2. Purkinje cells have a single long axon that forms an inhibitory projection to the cerebellar nuclei (Paul & Limaiem, 2023) and they strongly express $\alpha_2\delta$-2 mRNA (Barclay et al., 2001). Hence, modulating the trans-synaptic signaling with postsynaptic $GABA_AR$, for example, by the p.R596P mutation of $\alpha_2\delta$-2, may lead to a decreased functionality of this inhibitory GABAergic projection. Subsequently, this can lead to an excitatory–inhibitory imbalance which may ultimately underlie the epileptic phenotype observed in the patients.

Recent findings suggest a pivotal and highly redundant role of presynaptic $\alpha_2\delta$ proteins in the formation and differentiation of glutamatergic synapses in CNS neurons (Ablinger et al., 2022; Schopf et al., 2021). Our present data show that expression of $\alpha_2\delta$-2_R596P in WT neurons endogenously expressing three $\alpha_2\delta$ isoforms ($\alpha_2\delta$-1-3) affects pre- and postsynaptic differentiation as indicated by reduced presynaptic synapsin clustering and smaller mEPSC amplitudes. This phenotype, although milder, resembles the defect in synaptic differentiation observed in $\alpha_2\delta$ triple-knockout/knockdown neurons

(Schopf et al., 2021). $\alpha_2\delta$ proteins homologously expressed in hippocampal neurons must compete with endogenously expressed $\alpha_2\delta$ isoforms. Hence, the altered consequences of expressing mutated $\alpha_2\delta$-2 in comparison with WT $\alpha_2\delta$-2, such as defective pre- and subsequently postsynaptic differentiation, indicate a dominant-negative effect. Even more so as total neuronal surface expression is strongly affected by the p.R596P mutation. A similar situation may occur in the patients harboring the recessive p.R596P mutation: since $\alpha_2\delta$-2 is the dominating cerebellar isoform and both patients were found to be homozygous for the mutation, synapse differentiation may be affected by the dominant negative behavior of the mutated $\alpha_2\delta$-2 protein in competition with the remaining endogenous $\alpha_2\delta$ isoforms 1 and 3.

The negative effect of homologous $\alpha_2\delta$-2_R596P expression on the amplitudes of mEPSCs is an interesting observation by itself. The reduced synapsin content upon expression of mutated $\alpha_2\delta$-2 may indicate a defect in presynaptic vesicle recruitment and hence may contribute to a smaller amount of neurotransmitter release in response to spontaneous Ca^{2+} influx, which leads to a reduced response of postsynaptic AMPA receptor. Alternatively and given the pivotal role of presynaptic $\alpha_2\delta$ for both pre- and postsynaptic differentiation and the identified trans-synaptic functions of $\alpha_2\delta$ isoforms (Ablinger et al., 2022; Fell et al., 2016; Geisler et al., 2019), p.R596P may exert its deleterious effect via defective trans-synaptic signaling thereby changing the abundance of postsynaptic AMPA receptors.

Taken together, our data demonstrate three consequences of the p.R596P mutation on synaptic functions, which may only be partially related: first, reduced trans-synaptic recruitment of $GABA_AR$; second, reduced presynaptic synapsin clustering in glutamatergic nerve terminals; and third, reduced amplitudes of mEPSCs.

4.4 | Potential disease mechanisms

The functional characterization of the bi-allelic mutation p.R596P in $\alpha_2\delta$-2 provides three possible mechanistic explanations for how a defective $\alpha_2\delta$-2 protein could be linked to DEE. Firstly, mutations in $\alpha_2\delta$-2 can affect its role as a VGCC subunit and disrupt channel-dependent functions in an isoform- (differential effects on $Ca_V1.3$ L-type and $Ca_V2.1$ P/Q-type channels) and tissue-specific (presynaptic abundance of $Ca_V2.1$) manner. Either way, normal Ca^{2+} handling in pre- and postsynaptic compartments will be affected. Secondly, the reduced trans-synaptic coupling to postsynaptic $GABA_ARs$ accompanying the low membrane expression of $\alpha_2\delta$-2_R596P may reduce the functionality of GABAergic inhibitory synapses, which is of relevance for the predominant expression of $\alpha_2\delta$-2 in the cerebellum. Thirdly, the reduction in presynaptic clustering of synapsin and the amplitude of mEPSCs are indications of aberrant synaptic differentiation which decreases the probability of neurotransmitter release and weakens synaptic connectivity. All these proposed pathophysiological mechanisms may ultimately lead to an aberrant excitatory–inhibitory balance that underlies DEEs and, more broadly, neurodevelopmental disorders. Moreover, our study emphasizes the importance of studying the consequences of disease-associated $\alpha_2\delta$ protein mutations on both the classical functions as VGCC subunits and synaptic functions.

AUTHOR CONTRIBUTIONS

Sabrin Haddad: Funding acquisition; investigation; conceptualization; writing – original draft; methodology; writing – review and editing. **Cornelia Ablinger:** Software; conceptualization; methodology; writing – review and editing; investigation. **Ruslan Stanika:** Conceptualization; investigation; methodology; writing – review and editing; supervision. **Manuel Hessenberger:** Conceptualization; investigation; methodology; visualization; writing – review and editing; supervision. **Marta Campiglio:** Investigation; methodology; writing – review and editing; supervision. **Nadine J. Ortner:** Supervision; methodology; conceptualization; writing – review and editing. **Petronel Tuluc:** Conceptualization; supervision; writing – review and editing; methodology. **Gerald J. Obermair:** Conceptualization; funding acquisition; writing – review and editing; writing – original draft; methodology; project administration; supervision; resources.

ACKNOWLEDGMENTS

This work was supported by grants from the Austrian Science Fund (DOC30 to G.J.O., P35087 to N.J.O., P31434, P36053, and DOC178 to P.T.) and the Gesellschaft füsr Forschungsförderung Niederösterreich (LSC19-017 to G.J.O. and FTI22-D-013 to S.H.). We thank Anja Beierfuß and her team for animal care. We acknowledge support by the Open Access Publishing Fund of Karl Landsteiner University of Health Sciences, Krems, Austria. This work is part of the doctoral thesis of S.H.

CONFLICT OF INTEREST STATEMENT

The authors declare no competing financial interests.

PEER REVIEW

The peer review history for this article is available at https://www.webofscience.com/api/gateway/wos/peer-review/10.1111/jnc.16197.

DATA AVAILABILITY STATEMENT

Not applicable or already included in the manuscript.

ORCID

Gerald J. Obermair https://orcid.org/0000-0003-0005-8563

REFERENCES

Ablinger, C., Eibl, C., Geisler, S. M., Campiglio, M., Stephens, G. J., Missler, M., & Obermair, G. J. (2022). $\alpha_2\delta$-4 and Cachd1 proteins are regulators of presynaptic functions. *International Journal of Molecular Sciences*, *23*, 9885.

Ablinger, C., Eibl, C., Roznovcova, M., Cottrell, G. S., Stephens, G. J., & Obermair, G. J. (2024). The presynaptic α2δ protein family and their therapeutic potential. In G. Stephens & E. Stevens (Eds.), *Ion*

channels as targets in drug discovery (pp. 57–89). Springer. https://doi.org/10.1007/978-3-031-52197-3_3

Ablinger, C., Geisler, S. M., Stanika, R. I., Klein, C. T., & Obermair, G. J. (2020). Neuronal $\alpha_2\delta$ proteins and brain disorders. *Pflügers Archiv*, *472*, 845–863.

Barclay, J., Balaguero, N., Mione, M., Ackerman, S. L., Letts, V. A., Brodbeck, J., Canti, C., Meir, A., Page, K. M., Kusumi, K., Perez-Reyes, E., Lander, E. S., Frankel, W. N., Gardiner, R. M., Dolphin, A. C., & Rees, M. (2001). Ducky mouse phenotype of epilepsy and ataxia is associated with mutations in the Cacna2d2 gene and decreased calcium channel current in cerebellar Purkinje cells. *The Journal of Neuroscience*, *21*, 6095–6104.

Beeson, K. A., Beeson, R., Westbrook, G. L., & Schnell, E. (2020). $\alpha 2\delta$-2 Protein controls structure and function at the cerebellar climbing fiber synapse. *The Journal of Neuroscience*, *40*(12), 2403–2415. https://doi.org/10.1523/jneurosci.1514-19.2020

Beeson, K. A., Westbrook, G. L., & Schnell, E. (2021). $\alpha 2\delta$-2 is required for depolarization-induced suppression of excitation in Purkinje cells. *The Journal of Physiology*, *600*(1), 111–122. https://doi.org/10.1113/jp282438

Bozarth, X., Dines, J. N., Cong, Q., Mirzaa, G. M., Foss, K., Lawrence Merritt, J., Thies, J., Mefford, H. C., & Novotny, E. (2018). Expanding clinical phenotype in CACNA1C related disorders: From neonatal onset severe epileptic encephalopathy to late-onset epilepsy. *American Journal of Medical Genetics. Part A*, *176*, 2733–2739.

Brockhaus, J., Bruggen, B., & Missler, M. (2019). Imaging and analysis of presynaptic calcium influx in cultured neurons using synGCaMP6f. *Frontiers in Synaptic Neuroscience*, *11*, 12.

Brodbeck, J., Davies, A., Courtney, J. M., Meir, A., Balaguero, N., Canti, C., Moss, F. J., Page, K. M., Pratt, W. S., Hunt, S. P., Barclay, J., Rees, M., & Dolphin, A. C. (2002). The ducky mutation in Cacna2d2 results in altered Purkinje cell morphology and is associated with the expression of a truncated $\alpha_2\delta$-2 protein with abnormal function. *The Journal of Biological Chemistry*, *277*, 7684–7693.

Butler, K. M., Holt, P. J., Milla, S. S., da Silva, C., Alexander, J. J., & Escayg, A. (2018). Epileptic encephalopathy and cerebellar atrophy resulting from compound heterozygous CACNA2D2 variants. *Case Reports in Genetics*, *2018*, 6308283.

Canti, C., Nieto-Rostro, M., Foucault, I., Heblich, F., Wratten, J., Richards, M. W., Hendrich, J., Douglas, L., Page, K. M., Davies, A., & Dolphin, A. C. (2005). The metal-ion-dependent adhesion site in the Von Willebrand factor-a domain of $\alpha_2\delta$ subunits is key to trafficking voltage-gated Ca^{2+} channels. *Proceedings of the National Academy of Sciences of the United States of America*, *102*, 11230–11235.

Cao, Y. Q., Piedras-Renteria, E. S., Smith, G. B., Chen, G., Harata, N. C., & Tsien, R. W. (2004). Presynaptic Ca^{2+} channels compete for channel type-preferring slots in altered neurotransmission arising from Ca^{2+} channelopathy. *Neuron*, *43*, 387–400.

Cassidy, J. S., Ferron, L., Kadurin, I., Pratt, W. S., & Dolphin, A. C. (2014). Functional exofacially tagged N-type calcium channels elucidate the interaction with auxiliary $\alpha_2\delta$-1 subunits. *Proceedings of the National Academy of Sciences of the United States of America*, *111*, 8979–8984.

Castellano, A., Wei, X., Birnbaumer, L., & Perez-Reyes, E. (1993). Cloning and expression of a third calcium channel beta subunit. *The Journal of Biological Chemistry*, *268*, 3450–3455.

Dahimene, S., von Elsner, L., Holling, T., Mattas, L. S., Pickard, J., Lessel, D., Pilch, K. S., Kadurin, I., Pratt, W. S., Zhulin, I. B., Dai, H., Hempel, M., Ruzhnikov, M. R. Z., Kutsche, K., & Dolphin, A. C. (2022). Biallelic CACNA2D1 loss-of-function variants cause early-onset developmental epileptic encephalopathy. *Brain*, *145*, 2721–2729.

Davies, A., Hendrich, J., Van Minh, A. T., Wratten, J., Douglas, L., & Dolphin, A. C. (2007). Functional biology of the $\alpha_2\delta$ subunits of voltage-gated calcium channels. *Trends in Pharmacological Sciences*, *28*, 220–228.

Di Biase, V., Flucher, B. E., & Obermair, G. J. (2009). Resolving subsynaptic compartments with double immunofluorescence labeling in hippocampal neurons. *Journal of Neuroscience Methods*, *176*, 78–84.

Dolphin, A. C. (2016). Voltage-gated calcium channels and their auxiliary subunits: Physiology and pathophysiology and pharmacology. *The Journal of Physiology*, *594*, 5369–5390.

Dolphin, A. C., & Obermair, G. J. (2022). Regulation of calcium channels and synaptic function by auxiliary $\alpha_2\delta$ subunits. In G. W. Zamponi & N. Weiss (Eds.), *Voltage-Gated Calcium Channels* (pp. 93–114). Springer International Publishing.

Donato, R., Page, K. M., Koch, D., Nieto-Rostro, M., Foucault, I., Davies, A., Wilkinson, T., Rees, M., Edwards, F. A., & Dolphin, A. C. (2006). The ducky(2J) mutation in Cacna2d2 results in reduced spontaneous Purkinje cell activity and altered gene expression. *The Journal of Neuroscience*, *26*, 12576–12586.

Edvardson, S., Oz, S., Abulhijaa, F. A., Taher, F. B., Shaag, A., Zenvirt, S., Dascal, N., & Elpeleg, O. (2013). Early infantile epileptic encephalopathy associated with a high voltage gated calcium channelopathy. *Journal of Medical Genetics*, *50*, 118–123.

Epi, K. C. (2016). De novo mutations in SLC1A2 and CACNA1A are important causes of epileptic encephalopathies. *American Journal of Human Genetics*, *99*, 287–298.

Epi, K. C., Epilepsy Phenome/Genome Project, Allen, A. S., Berkovic, S. F., Cossette, P., Delanty, N., Dlugos, D., Eichler, E. E., Epstein, M. P., Glauser, T., Goldstein, D. B., Han, Y., Heinzen, E. L., Hitomi, Y., Howell, K. B., Johnson, M. R., Kuzniecky, R., Lowenstein, D. H., Lu, Y. F., … Winawer, M. R. (2013). De novo mutations in epileptic encephalopathies. *Nature*, *501*, 217–221.

Etemad, S., Obermair, G. J., Bindreither, D., Benedetti, A., Stanika, R., di Biase, V., Burtscher, V., Koschak, A., Kofler, R., Geley, S., Wille, A., Lusser, A., Flockerzi, V., & Flucher, B. E. (2014). Differential neuronal targeting of a new and two known calcium channel β_4 subunit splice variants correlates with their regulation of gene expression. *The Journal of Neuroscience*, *34*, 1446–1461.

Fell, B., Eckrich, S., Blum, K., Eckrich, T., Hecker, D., Obermair, G. J., Münkner, S., Flockerzi, V., Schick, B., & Engel, J. (2016). $\alpha_2\delta 2$ controls the function and trans-synaptic coupling of Cav1.3 channels in mouse inner hair cells and is essential for Normal hearing. *The Journal of Neuroscience*, *36*, 11024–11036.

Folci, A., Steinberger, A., Lee, B., Stanika, R., Scheruebel, S., Campiglio, M., Ramprecht, C., Pelzmann, B., Hell, J. W., Obermair, G. J., Heine, M., & di Biase, V. (2018). Molecular mimicking of C-terminal phosphorylation tunes the surface dynamics of Ca(V)1.2 calcium channels in hippocampal neurons. *The Journal of Biological Chemistry*, *293*, 1040–1053.

Geisler, S., Schopf, C. L., & Obermair, G. J. (2015). Emerging evidence for specific neuronal functions of auxiliary calcium channel $\alpha_2\delta$ subunits. *General Physiology and Biophysics*, *34*, 105–118.

Geisler, S., Schopf, C. L., Stanika, R., Kalb, M., Campiglio, M., Repetto, D., Traxler, L., Missler, M., & Obermair, G. J. (2019). Presynaptic $\alpha_2\delta$-2 Calcium Channel subunits regulate postsynaptic GABA(a) receptor abundance and axonal wiring. *The Journal of Neuroscience*, *39*, 2581–2605.

Gong, H. C., Hang, J., Kohler, W., Li, L., & Su, T. Z. (2001). Tissue-specific expression and gabapentin-binding properties of calcium channel $\alpha_2\delta$ subunit subtypes. *The Journal of Membrane Biology*, *184*, 35–43.

Helbig, K. L., Lauerer, R. J., Bahr, J. C., Souza, I. A., Myers, C. T., Uysal, B., Schwarz, N., Gandini, M. A., Huang, S., Keren, B., Mignot, C., Afenjar, A., Billette de Villemeur, T., Héron, D., Nava, C., Valence, S., Buratti, J., Fagerberg, C. R., Soerensen, K. P., … Wiener, J. (2018). De novo pathogenic variants in CACNA1E cause developmental and epileptic encephalopathy with contractures, macrocephaly, and Dyskinesias. *American Journal of Human Genetics*, *103*, 666–678.

Hessenberger, M., Haddad, S., & Obermair, G. J. (2023). Pathophysiological roles of auxiliary calcium channel $\alpha_2\delta$ subunits. In J. Striessnig (Ed.), *Voltage-gated Ca^{2+} channels: Pharmacology, modulation and their role in human disease. Handbook of Experimental Pharmacology, volume 279* (pp. 289–316). Springer.

Hoppa, M. B., Lana, B., Margas, W., Dolphin, A. C., & Ryan, T. A. (2012). $\alpha_2\delta$ expression sets presynaptic calcium channel abundance and release probability. *Nature*, *486*, 122–125.

Ivanov, S. V., Ward, J. M., Tessarollo, L., McAreavey, D., Sachdev, V., Fananapazir, L., Banks, M. K., Morris, N., Djurickovic, D., Devor-Henneman, D. E., Wei, M. H., Alvord, G. W., Gao, B., Richardson, J. A., Minna, J. D., Rogawski, M. A., & Lerman, M. I. (2004). Cerebellar ataxia, seizures, premature death, and cardiac abnormalities in mice with targeted disruption of the Cacna2d2 gene. *The American Journal of Pathology*, *165*, 1007–1018.

Jumper, J., Evans, R., Pritzel, A., Green, T., Figurnov, M., Ronneberger, O., Tunyasuvunakool, K., Bates, R., Žídek, A., Potapenko, A., Bridgland, A., Meyer, C., Kohl, S. A. A., Ballard, A. J., Cowie, A., Romera-Paredes, B., Nikolov, S., Jain, R., Adler, J., … Hassabis, D. (2021). Highly accurate protein structure prediction with AlphaFold. *Nature*, *596*, 583–589.

Kaech, S., & Banker, G. (2006). Culturing hippocampal neurons. *Nature Protocols*, *1*, 2406–2415.

Koschak, A., Reimer, D., Huber, I., Grabner, M., Glossmann, H., Engel, J., & Striessnig, J. (2001). Alpha 1D (Cav1.3) subunits can form l-type Ca^{2+} channels activating at negative voltages. *The Journal of Biological Chemistry*, *276*, 22100–22106.

Mullner, C., Broos, L. A., van den Maagdenberg, A. M., & Striessnig, J. (2004). Familial hemiplegic migraine type 1 mutations K1336E, W1684R, and V1696I alter Cav2.1 Ca^{2+} channel gating: Evidence for beta-subunit isoform-specific effects. *The Journal of Biological Chemistry*, *279*, 51844–51850.

Niu, X., Yang, Y., Chen, Y., Cheng, M., Liu, M., Ding, C., Tian, X., Yang, Z., Jiang, Y., & Zhang, Y. (2022). Genotype-phenotype correlation of CACNA1A variants in children with epilepsy. *Developmental Medicine and Child Neurology*, *64*, 105–111.

Obermair, G. J., Kugler, G., Baumgartner, S., Tuluc, P., Grabner, M., & Flucher, B. E. (2005). The Ca^{2+} channel $\alpha_2\delta$-1 subunit determines Ca^{2+} current kinetics in skeletal muscle but not targeting of α1S or excitation-contraction coupling. *The Journal of Biological Chemistry*, *280*, 2229–2237.

Obermair, G. J., Szabo, Z., Bourinet, E., & Flucher, B. E. (2004). Differential targeting of the L-type Ca^{2+} channel alpha 1C (CaV1.2) to synaptic and extrasynaptic compartments in hippocampal neurons. *The European Journal of Neuroscience*, *19*, 2109–2122.

Obermair, G. J., Tuluc, P., & Flucher, B. E. (2008). Auxiliary Ca^{2+} channel subunits: Lessons learned from muscle. *Current Opinion in Pharmacology*, *8*, 311–318.

Paul, M. S., & Limaiem, F. (2023). Histology, Purkinje cells. In: *StatPearls*. Treasure Island (FL).

Pippucci, T., Parmeggiani, A., Palombo, F., Maresca, A., Angius, A., Crisponi, L., Cucca, F., Liguori, R., Valentino, M. L., Seri, M., & Carelli, V. (2013). A novel null homozygous mutation confirms CACNA2D2 as a gene mutated in epileptic encephalopathy. *PLoS One*, *8*, e82154.

Punetha, J., Karaca, E., Gezdirici, A., Lamont, R. E., Pehlivan, D., Marafi, D., Appendino, J. P., Hunter, J. V., Akdemir, Z. C., Fatih, J. M., Jhangiani, S. N., Gibbs, R. A., Innes, A. M., Posey, J. E., & Lupski, J. R. (2019). Biallelic CACNA2D2 variants in epileptic encephalopathy and cerebellar atrophy. *Annals of Clinical Translational Neurology*, *6*, 1395–1406.

Schlick, B., Flucher, B. E., & Obermair, G. J. (2010). Voltage-activated calcium channel expression profiles in mouse brain and cultured hippocampal neurons. *Neuroscience*, *167*, 786–798.

Schopf, C. L., Ablinger, C., Geisler, S. M., Stanika, R. I., Campiglio, M., Kaufmann, W. A., Nimmervoll, B., Schlick, B., Brockhaus, J., Missler, M., Shigemoto, R., & Obermair, G. J. (2021). Presynaptic $\alpha_2\delta$ subunits are key organizers of glutamatergic synapses. *Proceedings of the National Academy of Sciences of the United States of America*, *118*(14), e1920827118.

Schredelseker, J., Di Biase, V., Obermair, G. J., Felder, E. T., Flucher, B. E., Franzini-Armstrong, C., & Grabner, M. (2005). The β_{1a} subunit is essential for the assembly of dihydropyridine-receptor arrays in skeletal muscle. *Proceedings of the National Academy of Sciences of the United States of America*, *102*, 17219–17224.

Scott, M. B., & Kammermeier, P. J. (2017). Ca(V)2 channel subtype expression in rat sympathetic neurons is selectively regulated by $\alpha_2\delta$ subunits. *Channels*, *11*, 555–573.

Stanika, R., Campiglio, M., Pinggera, A., Lee, A., Striessnig, J., Flucher, B. E., & Obermair, G. J. (2016). Splice variants of the Ca(V)1.3 L-type calcium channel regulate dendritic spine morphology. *Scientific Reports*, *6*, 34528.

Tuluc, P., Kern, G., Obermair, G. J., & Flucher, B. E. (2007). Computer modeling of siRNA knockdown effects indicates an essential role of the Ca^{2+} channel $\alpha_2\delta$-1 subunit in cardiac excitation-contraction coupling. *Proceedings of the National Academy of Sciences of the United States of America*, *104*, 11091–11096.

Varadi, M., Anyango, S., Deshpande, M., Nair, S., Natassia, C., Yordanova, G., Yuan, D., Stroe, O., Wood, G., Laydon, A., Žídek, A., Green, T., Tunyasuvunakool, K., Petersen, S., Jumper, J., Clancy, E., Green, R., Vora, A., Lutfi, M., … Velankar, S. (2022). AlphaFold protein structure database: Massively expanding the structural coverage of protein-sequence space with high-accuracy models. *Nucleic Acids Research*, *50*, D439–D444.

Vembar, S. S., & Brodsky, J. L. (2008). One step at a time: Endoplasmic reticulum-associated degradation. *Nature Reviews. Molecular Cell Biology*, *9*, 944–957.

Voigt, A., Freund, R., Heck, J., Missler, M., Obermair, G. J., Thomas, U., & Heine, M. (2016). Dynamic association of calcium channel subunits at the cellular membrane. *Neurophotonics*, *3*, 041809.

How to cite this article: Haddad, S., Ablinger, C., Stanika, R., Hessenberger, M., Campiglio, M., Ortner, N. J., Tuluc, P., & Obermair, G. J. (2025). A biallelic mutation in CACNA2D2 associated with developmental and epileptic encephalopathy affects calcium channel-dependent as well as synaptic functions of $\alpha_2\delta$-2. *Journal of Neurochemistry*, *169*, e16197. https://doi.org/10.1111/jnc.16197